An Imaging and Spectroscopic Exploration of the Dusty Compact Obscured Nucleus Galaxy Zw 049.057

The Astrophysical Journal Supplement Series, 274:3 (20pp), 2024 September https://doi.org/10.3847/1538-4365/ad55c9

An Imaging and Spectroscopic Exploration of the Dusty Compact Obscured Nucleus Galaxy Zw 049.057*

J. S. Gallagher[1,8], R. Kotulla[1], L. Laufman[2], E. Geist[1], S. Aalto[3], N. Falstad[3], S. König[3], J. Krause[4], G. C. Privon[5,9,10], C. Wethers[3], A. Evans[5,6], and M. Gorski[7]
[1] Department of Astronomy, University of Wisconsin-Madison, 475 N Charter Street, Madison, WI 53706, USA
[2] School of Physics and Astronomy, 116 Church Street SE, Minneapolis, MN 55455, USA
[3] Department of Space, Earth and Environment, Chalmers University of Technology, Onsala Space Observatory, 439 92 Onsala, Sweden
[4] Space Telescope Science Institute, 3700 San Martin Drive, Baltimore, MD 21218, USA
[5] National Radio Astronomy Observatory, 520 Edgemont Road, Charlottesville, VA 22903, USA
[6] Department of Astronomy, 530 McCormick Road, University of Virginia, Charlottesville, VA 22904, USA
[7] Center for Interdisciplinary Exploration and Research in Astrophysics, Northwestern University, 1800 Sherman Avenue, Evanston, IL 60201, USA
Received 2023 November 27; revised 2024 June 6; accepted 2024 June 6; published 2024 August 12

Abstract

Zw 049.057 is a moderate-mass, dusty, early-type galaxy that hosts a powerful compact obscured nucleus (CON, $L_{\rm FIR,CON} \geqslant 10^{11}\,L_{\odot}$). The resolution of the Hubble Space Telescope enabled measurements of the stellar light distribution and characterization of dust features. Zw 049.057 is inclined with a prominent three-zone disk; the $R \approx 1$ kpc star-forming inner dusty disk contains molecular gas, a main disk with less dust and an older stellar population, and a newly detected outer stellar region at $R > 6$ kpc with circular isophotes. Previously unknown polar dust lanes are signatures of a past minor merger that could have warped the outer disk to near face-on. Dust transmission measurements provide lower limit gas mass estimates for dust features. An extended region with moderate optical depth and $M \geqslant 2 \times 10^{8}\,M_{\odot}$ obscures the central 2 kpc. Optical spectra show strong interstellar Na D absorption with a constant velocity across the main disk, likely arising in this extraplanar medium. Opacity measurements of the two linear dust features, pillars, give a total mass of $\geqslant 10^{6}\,M_{\odot}$, flow rates of $\geqslant 2\,M_{\odot}\,{\rm yr}^{-1}$, and few Myr flow times. Dust pillars are associated with the CON and are visible signs of its role in driving large-scale feedback. Our assessments of feedback processes suggest gas recycling sustains the CON. However, radiation pressure driven mass loss and efficient star formation must be avoided for the active galactic nucleus to retain sufficient gas over its lifespan to produce substantial mass growth of the central black hole.

Unified Astronomy Thesaurus concepts: Galaxy evolution (594); Interstellar dust (836); Active galaxies (17); Galaxy mergers (608); Galaxy photometry (611); Galaxy spectroscopy (2171); Galaxy processes (614)

1. Introduction

The development of the baryonic components of galaxies involves the coevolution of central supermassive black holes (SMBHs) with the stellar galactic bodies. These processes involve feedback from active galactic nuclei (AGNs) that can remove gas via a variety of processes in concert with mass inflows that feed growth of the central black holes and power AGNs. Galaxies with compact obscured nuclei (CONs) are systems with extraordinary central concentrations of dusty interstellar matter within radii of $\lesssim$100 pc (see Evans et al. 2003; Sakamoto et al. 2010; Aalto et al. 2015, 2020; Martín et al. 2016; Privon et al. 2017; Scoville et al. 2017; Falstad et al. 2021; Donnan et al. 2023; Gorski et al. 2023). Gas columns in CONs are $\sim 10^{25}\,{\rm cm}^{-2}$, which obscures nuclear emission across the spectrum, extending from X-rays to millimeter wavelengths. Therefore, CONs offer insights into nuclear growth and feedback under extreme conditions where the immediately surrounding gas reservoirs are unusually dense and massive. Due to their high luminosities, CONs expel dense, dusty gas that absorbs background galaxy light. Spatially extended dusty gas produced by these dramatic feedback processes can be observed with the Hubble Space Telescope (HST) in absorption at gas column densities and spatial scales that are difficult to access via other methods.

The CON host Zw 049.057 is an inclined early-type galaxy with an inner dusty star-forming disk (Martin et al. 1988; Scoville et al. 2000; Alonso-Herrero et al. 2006). This galaxy was cataloged on blue-sensitive photographic plates by Zwicky, who characterized it as a compact early-type galaxy. Later ground-based imaging and spectroscopy led to the classification of Zw 049.057 as a noninteracting starburst galaxy (e.g., Poggianti & Wu 2000; Hattori et al. 2004; Alonso-Herrero et al. 2006; Stierwalt et al. 2013; Larson et al. 2016). Observations of the global H I 21 cm line profile revealed that Zw 049.057 belongs to the rare group of luminous infrared galaxies (LIRGs) where H I is in absorption (Baan et al. 1987; Mirabel & Sanders 1988; Morganti & Oosterloo 2018). Following the IRAS detection of Zw 049.057 as an LIRG (Soifer et al. 1987), the galaxy attracted interest in terms of its molecular content, including early detection as an OH maser source (Baan et al. 1987). Improved millimeter and submillimeter observations demonstrated the extreme nature of

* Based in part on observations obtained with the Southern African Large Telescope (SALT).
[8] Department of Physics, Macalester College, 1600 Grand Avenue, St. Paul, MN 55105, USA.
[9] Department of Astronomy, 530 McCormick Road, University of Virginia, Charlottesville, VA 22904, USA.
[10] Department of Astronomy, University of Florida, P. O. Box 112055, Gainesville, FL 32611, USA.

the central molecular gas component of Zw 049.057 (Baan et al. 1987; Planesas et al. 1991; Baan et al. 2008). Similarly, a variety of observations established that the central molecular medium contains high-density molecular matter (Mangum et al. 2008; Papadopoulos et al. 2012; Mangum et al. 2013a; Baan et al. 2017; Herrero-Illana et al. 2019), which includes a warm component with temperatures of ≈150 K (Mangum et al. 2013b; Petric et al. 2018), along with evidence for even hotter dust components (González-Alfonso & Sakamoto 2019; Baba et al. 2022).

High angular resolution observations with millimeter/submillimeter interferometers provide superb information on properties of the dense, bright nuclear regions, and demonstrate that emission from CONs provide a substantial fraction of the host galaxies' bolometric luminosities (Costagliola et al. 2015; Privon et al. 2017; González-Alfonso & Sakamoto 2019; Falstad et al. 2021; Baba et al. 2022; García-Bernete et al. 2022). Due to the extreme opacities of CONs, the nature of their power sources is unclear, and AGNs, extreme starbursts, or gravitational energy from gas accreting into the CON are options (Aalto et al. 2015, 2019, 2020; Gorski et al. 2024). Although classic ultraluminous infrared galaxy (ULIRG) CONs, such as that in Arp 220, are associated with ongoing mergers, the evolutionary channels leading to CONs in LIRGs are not fully understood. About 30% of ULIRGs and 10%–20% of the surveyed LIRGs contain CONs (Falstad et al. 2021; Donnan et al. 2023; Nishimura et al. 2024). In this paper we present a study of the optical structure of the LIRG CON Zw 049.057 (CGCG 049-057, PGC054330; $D = 59$ Mpc, $L_{\rm FIR} \approx 11.5 \pm 0.1\ L_{\odot}$; Aalto et al. 2015; Falstad et al. 2015). Due to its orientation and relative proximity, Zw 049.057 is an excellent target for exploring connections between a CON and its host galaxy.

At optical wavelengths, Zw 049.05 stands out due to the presence of prominent dust absorption features along the minor axis that were seen in the ground-based images by Martin et al. (1988) and later confirmed using HST by Scoville et al. (2000). The minor axis dust features in Zw 049.057 contrast with most early-type disk galaxies (e.g., types S0 or S0/a) where dust absorption is largely confined to disks, either in the central regions or appearing as filaments due to disk warps (e.g., Tran et al. 2001; Keel et al. 2015; Boizelle et al. 2017). The most prominent dust features, two narrow "dust pillars,"[11] connect to the central regions of Zw 049.057 (Scoville et al. 2000) tracing ongoing gas outflows and feedback associated with its nuclear region. Zw 049.057 is a CON host galaxy that also is in the midst of a galactic-scale dust storm.

Observations obtained with the Herschel observatory added to the initial evidence for a massive warm, dense central molecular component and associated molecular wind in Zw 049.057 (Greve et al. 2014; Rosenberg et al. 2015; Kamenetzky et al. 2017; Lu et al. 2017). Molecular line spectra obtained by Aalto et al. (2015) revealed significant emission from vibrationally excited nuclear HCN emission from a warm, dense, and optically thick molecular medium, which is the primary observational signature of a CON (e.g., Imanishi & Nakanishi 2013; Aalto et al. 2015; Falstad et al. 2021; Sakamoto et al. 2021; Nishimura et al. 2024). Falstad et al. (2015) also showed that the HCN emission arises from a very compact central region with a high gas column density, and Falstad et al. (2018) detected a nuclear molecular wind. González-Alfonso & Sakamoto (2019) quantitatively interpreted the infrared and molecular line observations of Zw 049.057 with a radiative transfer model for the optically thick central dusty region. Their model yields a size of 15–25 pc for the deeply obscured region that provides ∼1/3–1/2 of $L_{\rm FIR}$ in Zw 049.057. The nucleus is behind an H_2 column density of $\log_{10}(N(H_2)) \simeq 10^{24.8}$ cm^{-2} that yields an atomic H gas column density of $N_{\rm H} \simeq 10^{25.1}$ cm^{-2}, giving an interstellar medium (ISM) mass surface density toward the nucleus of an impressive ∼20 g cm^{-2}. Subarcsecond radio continuum observations by Song et al. (2022) penetrate the dense nuclear gas and dust envelope to reveal a compact continuum source that is consistent with the presence of an AGN within the Zw 049.057 CON.

We selected Zw 049.057 for a detailed exploration of the properties of a CON host galaxy due to its proximity and extensive set of existing multiwavelength observations. Our study focused on defining relationships between the Zw 049.057 CON and its galactic surroundings by assessing the properties of the extensive dust absorption features using images obtained with the Wide Field Camera 3 (WFC3) on HST. By mapping the distribution of dust absorption in structures extending outward from the central regions, we investigated connections between the subkiloparsec molecular outflows from the CON and larger kiloparsec-scale gas structures outlined by dust absorption. These data also allowed us to search for and find evidence of a recent minor merger. A spectrum obtained with the South African Large Telescope (SALT) enabled us to undertake an initial study of the kinematics of ionized gas in the dusty circumnuclear star-forming region. The spatial outward-inward organization of the paper is visually outlined in the upper panel of Figure 1, which includes labels for several of the major dust absorption features.

In Section 2 we review the observational material. The structure of the stellar components and stellar population properties of Zw 049.057 are discussed along with its local environment in Section 3. In Section 4, properties of the dust features are analyzed. Section 5 describes the emission-line properties of the inner region of Zw 049.057 where a high star formation rate (SFR) disk component is present. Section 6 explores properties of the nuclear region and the associated giant "dust pillars"—linear dust absorption features—that extend above the disk of Zw 049.057 (see Scoville et al. 2000). A discussion of our results in the context of evolution and feedback associated with the CON in Zw 049.057 is presented in Section 7, which leads to our conclusions in Section 8.

2. Observations

2.1. Hubble Space Telescope WFC3 Imaging

At ground-based resolution, optical images confirm Zw 049.057 is an S0/a system with asymmetrical dust obscuration above the disk to the north–northwest. The high-brightness central region stands out and is probably the basis for the Zwicky classification as a compact galaxy. Unfortunately this system is sufficiently distant that ground-based, seeing-limited images only provide a broad overview of its structure. We therefore obtained images of Zw 049.057 on 2017 March 5, using WFC3 on HST as a part of program GO-14278, PI J. S. Gallagher. At the distance of Zw 049.057, the WFC3 optical FWHM point-source resolution of 0.″07 corresponds to a linear scale of 20 pc. The observations are summarized in Table 1. The observations in this Table are available via MAST at doi:10.17909/GXFM-6061. Images in

[11] We use the term "pillar" to differentiate the linear central dust features in Zw 049.057 from more commonly observed dust filaments.

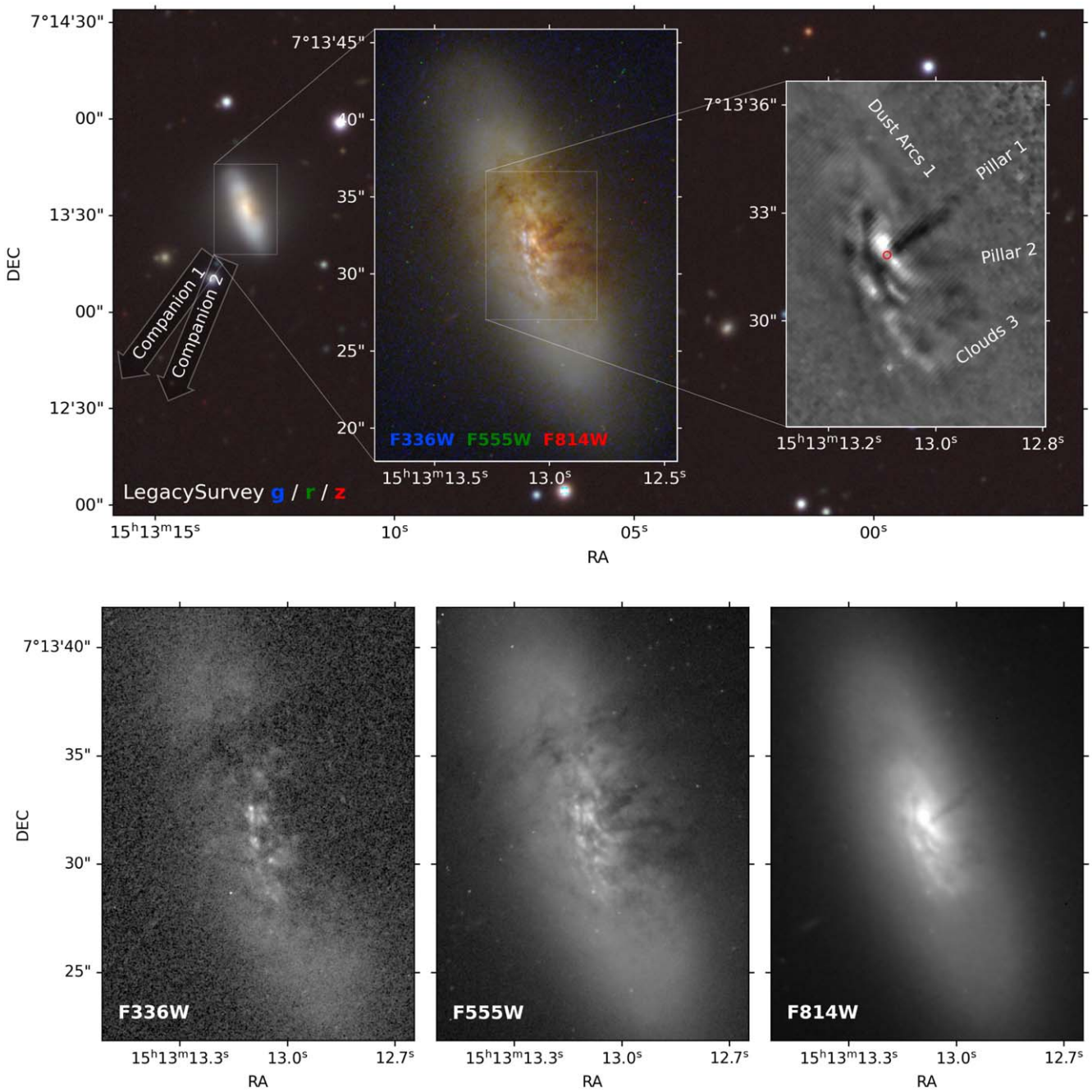

Figure 1. Upper panel: our approach in analyzing the properties of Zw 049.057. The images from left to right are from NOIRlab Legacy Survey's Sky Viewer (www.legacysurvey.org), our HST optical images, and a high-pass smoothed version of our F125W HST *J*-band image. The arrows in the left panel point to the southeasterly locations of the Zw 049.057 low-luminosity companions. Dust Pillars-1 and -2 make up the distinctive dust "V." The central image also shows the polar dust ring band crossing to the north of the central region. Our approach in this paper is to work from larger to smaller spatial scales, starting with the environment and global properties of Zw 049.057 and ending with characteristics of the nuclear region. The location of the CON is denoted by the red circle. Lower panel: the images in three filters illustrate effects of the decrease in optical depth with increasing wavelength. Diffuse dust complexes obscure much of the center of the galaxy in the HST F336W $U_{\rm HST}$ filter but are largely transparent in the F814W $I_{\rm HST}$ filter.

the three optical filters are shown in Figure 1. Using HST, we can study the ISM as traced by dust obscuration at gas column densities of $\sim 10^{21}$ cm^{-2} on spatial scales where molecular and dust emission is too faint to be readily measured with millimeter/submillimeter interferometers.[12]

We compared the coordinates on the original reduced WFC3 image frames to the Gaia reference frame using stars on the WFC3 chip 1 where the galaxy was observed and in the WFC3/IR channel. This comparison indicated coordinate offsets of several tenths of an arcsecond that are corrected in the latest versions of the WFC3/UVIS channel Zw 049.057 data in the MAST archive. Data with updated coordinates allowed us to determine the location of the nucleus and other features and to calibrate astrometric positions in the F125W image, where the archival image has offsets from the Gaia

[12] The James Webb Space Telescope offers the potential to map inner dust near- and mid-infrared emission with subarcsecond resolution for regions emitting polycyclic aromatic hydrocarbons or where dust is sufficiently warm (most likely to occur near the nucleus and in starbursting zones).

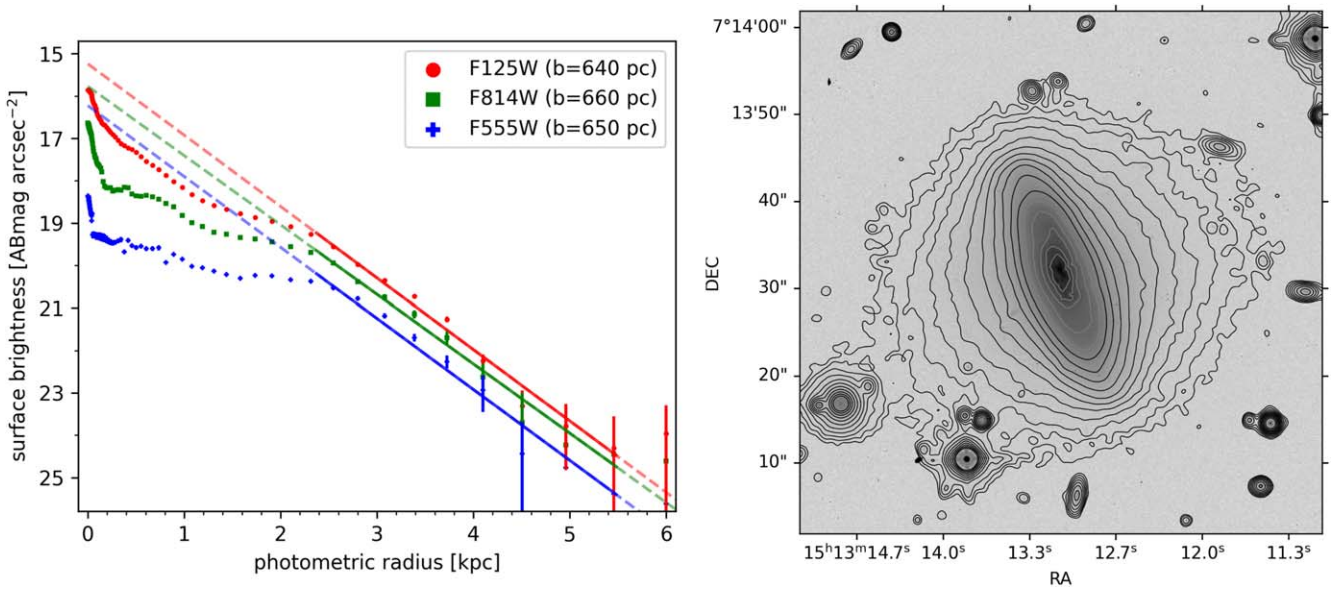

Figure 2. Results are shown from our isophotal analysis. Left panel: radial intensity plots are shown from ellipse fits to the HST images. The less-obscured outer disk regions show an exponential profile with a scale length of 2.″2 640 pc). The effects of dust obscuration result in all of the profiles overshooting the observed intensities within $R \lesssim 2$ kpc. The flatter intensity gradient at 6 kpc occurs in the region where the round outer light distribution begins to appear (see Section 3.2). Right: our WFC3 F125W image scaled to show the inclines inner disk of Zw 049.057 with a major axis position angle of 200° and nearly circular outer structure. The outermost isophotes are at $\mu_{\rm F125W,AB} \simeq 19$ mag arcsec^{-2}. We suggest that this feature is due to the presence of a warped outer disk associated with the interaction that produced the northern polar dust lane. The inner isophotes display the observed $b/a = 0.4$ axis ratio that we used to derive the inclination.

Table 1
WFC3 HST Observations of Zw 049.057

Filter	Channel	$T_{\rm expose}$ (s)	Data Set
F336W	WFC3/UVIS	2550	IDA603010
F555W	WFC3/UVIS	960	IDA603020
F814W	WFC3/UVIS	1000	IDA603030
F125W	WFC3/IR	306	IDA603040

reference frame. This comparison also showed that the original NICMOS of Scoville et al. (2000) images had a position offset of ∼0.″6 measured relative to WFC3 images with updated coordinates.

2.2. Spectroscopy

Red-region long-slit spectra along the major axis of Zw 049.057 were obtained with the Robert Stobie Spectrograph (RSS) on SALT (see Buckley et al. 2008) on UT dates 2019 March 15 and 28. The 1.″5 width slit was set to position angles of 18° for the major axis. We obtained two exposures of 1100 s with the PG1800 grating yielding a spectral resolution of 3100 at Hα derived from Gaussian fits to night sky OH lines with an angular scale of 0.″253 per 2 x 2 binned pixel. We estimate the seeing to have been ∼1.″3.

The SALT RSS PySALT pipeline[13] provided initial processed versions of the spectra to remove instrumental signatures (Crawford et al. 2010). Using IRAF, we combined the exposures, transformed the spectra to remove slit curvature, and applied a wavelength scale. We independently reduced each of the three CCDs in the RSS detector. Sky subtraction was done by selecting and combining regions above and below the area containing the signal from the galaxy that were subtracted from the signal area.

We checked our RSS wavelength calibrations against sky emission lines using wavelengths tabulated by Osterbrock et al. (1996). We incorporated wavelength offsets derived from the sky lines of -0.19 ± 0.05 Å for the Hα region and 0.23 Å for the Na D lines. We applied heliocentric corrections to our observed velocities using the IRAF rvcorrect routines.

3. Structure of the Stellar Body

3.1. The Disk

Figure 1 shows the complex optical structure of Zw 049.057. The main stellar disk has red colors and is crossed by multiple dust absorption features. Despite the dust, the inner disk is distinguished by enhanced surface brightness within $R_{\rm major} \approx 3''$ (860 pc). The inner disk is the site of intense star formation, producing strong emission lines in optical spectra (Section 5) and in narrowband imaging (Poggianti & Wu 2000; Alonso-Herrero et al. 2006). A UV-bright arm traces the eastern side of the inner disk. An inclination of 70° follows under the assumption that the main disk has an intrinsic axis ratio of $b/a = 0.2$ (see Holmberg 1958). The analysis by Scoville et al. (2000) based on NICMOS images provides information on the properties of the inner star-forming disk. Their F222M NICMOS data revealed the heavily obscured nuclear region at the center of the outer disk. Molecular material with a mass of $M_{\rm molec} = 1.6 \pm 0.2 \times 10^9\, M_\odot$ derived from CO 1–0 observations appears to be concentrated in the central part of the galaxy (Herrero-Illana et al. 2019). These observations do not fully sample the dense gas associated with the CON, but instead refer to gas in the central parts of the disk. We discuss the star-forming central disk of Zw 049.057 in more detail in Section 5.

Figure 2 shows results from ellipse fits to the intensity distributions in our HST images. The main disk (i.e., the region

[13] http://pysalt.salt.ac.za/

Table 2
Photometry of Zw 049.057

Property	Value	Notes
Magnitudes	$U_{336}(0) \lesssim 16.6$ $V_{555}(0) = 14.56$ $I_{814}(0) = 14.52$ $J_{125}(0) = 14.93$	STMAG, this study
$\log(L_\lambda/L_{\odot\lambda})$	HST-V: 9.6, HST-I: 9.8, HST-J:10.1, SST 3.6 μm 10.5	This study
Effective radius in kiloparsecs at λ	HST-J 1.3; SST 3.6 μm 0.9	SST less affected by dust

Note. Our HST *V*, *I*, *J* photometry has uncertainties at the 0.05 mag level and is in good agreement with ground-based data. The HST-*U*-band magnitude is an upper limit because the outer galaxy is not detected due to reduced surface brightness sensitivity in the F336W filter. The Galactic extinction correction is based on $A_V = 0.116$ and tabulated values for each filter from the NASA Extragalactic Database.

beyond a radius of roughly 1 kpc) is exponential with a scale length of 640 pc and major axis at a position angle of $200° \pm 2°$. The outer or main disk is symmetric with a relatively smooth optical structure, but intensities within $r \lesssim 1$ kpc are strongly affected in the optical bands by the ongoing galactic-scale dust storm. However, it is clear that the main disk in Zw 049.057 extends for nine radial exponential scale lengths and in this sense is not compact. The substantial central dust obscuration in Zw 049.057 leads to difficulties in obtaining unique model fits to the galaxy's image. We therefore characterized the size of Zw 049.057 by determining the effective (half-light) radius $R_e = 0.92$ kpc from an isophotal fit to the 3.6 μm Spitzer Space Telescope (SST) archival image (SSC & IRSA 2013). The measured R_e for Zw 049.057 decreases with increasing wavelength as the level of dust obscuration of the bright central region declines, so the 3.6 μm image provides the most reliable estimate of R_e.

The NASA Extragalactic Database gives $m_{\rm AB}(3.6\,\mu{\rm m}) = 13.54 \pm 0.1$, consistent with our photometry of an archival SST 3.6 μm image. For $D = 59$ Mpc, this yields $M_{\rm AB}(3.6) = -20.2$ and $L_{3.6} = 3 \pm 0.3 \times 10^{10}\,L_\odot$. Adopting a stellar mass-to-light ratio of $\gamma_{3.6}$, the stellar mass in Zw 049.057 is $M_* \approx 1.5 \times 10^{10}(\gamma_{3.6}/0.5)\,M_\odot$, consistent with the values found by U et al. (2012) and a factor of 2.5 greater than the mass derived by Leroy et al. (2019). Zw 049.057 is a moderate-mass galaxy, and we adopt $1.5 \times 10^{10}\,M_\odot$ for its stellar mass in the remainder of this paper. Stellar masses are especially useful for comparisons between galaxies as fundamental parameters and quantities that can be measured using a variety of techniques.

The photometric and structural properties of Zw 049.057 are summarized in Table 2. The far-infrared (FIR) luminosity of Zw 049.057 of $\log(L_{\rm IR}) = 11.5$ exceeds the stellar luminosity by a factor of 10. Since the bolometric luminosity in the dusty Z 049.057 system is essentially the same as $L_{\rm IR}$, then the observed stellar mass-to-light ratio of Zw 049.057 is $\gamma_{\rm tot,obs} = M_*/L_{\rm IR} \approx 0.05$. This value of $\gamma_{\rm tot,obs}$ is similar to values observed in extremely obscured ULIRGs, e.g., $\gamma_{\rm tot,obs} \approx 0.04$ for Arp 220 (see Chandar et al. 2023), but is more extreme than the $\gamma_{\rm tot,obs} \approx 0.2$ for the starbursting M82 system, which has one-third the stellar mass of Zw 049.057 (Leroy et al. 2019).

3.2. The Outer Stellar Component

While the main body of Zw 049.057 displays a disklike structure, at fainter levels of $\mu_{\rm F125W,STMAG} \geqslant 25$ mag arcsecond^{-2}, the isophotes trend toward being circular. This outer feature, illustrated in Figure 2, is also detected in the optical HST and ground-based images. Photometry along the southeastern major axis of the halo shows an approximately exponential light distribution with a scale length of $\approx 5''$ (1.4 kpc).

The three-dimensional form of the outer stellar region with circular isophotes is not clear. One possibility is a warped disk where the outer disk's line of nodes lies close to the current major axis of Zw 049.057. A warped outer disk would naturally account for the approximately exponential light distribution. Alternatively, this material could be a diffuse spheroidal stellar halo centered on the galaxy. If the symmetric light component is from a stellar halo, then this structure has a low degree of central mass concentration. Reflected light from the dusty outflow is another possibility, although this is inconsistent with the opening angles of the observed dust features. Therefore, we favor the warped, disklike stellar component interpretation.

Our images show the presence of polar dust arcs. Zw 049.057 experienced a recent minor merger that can induce disk warps (e.g., Sparke et al. 2009) and is in the late stage of a merger where the galaxy has not yet recovered its coplanar structure (see discussion in Section 6). Alternatively, a stellar halo could have an origin from stars lost during mergers. However, we do not detect the shells or streams in the round stellar component that are expected to persist for several Gyr after mergers (Oh et al. 2008; Eliche-Moral et al. 2018; Karademir et al. 2019). The absence of these features may be an observational limitation stemming from a combination of resolution and sensitivity, issues that could be addressed via deep imaging with the JWST.

Based on the present evidence of a merger that produced the polar dust lane (see Section 4), we prefer the warped disk model while recognizing that this interpretation requires that we observe Zw 049.057 from a special perspective. Given the likelihood that Zw 049.057 is the product of a galaxy–galaxy interaction, we searched the NASA ADS for companions. This revealed the apparently undisturbed pair of dwarf galaxies WISEA J151341.81+065603.6 and WISEA J151407.76 +065504.3 at redshift velocities of $v_{\rm helio} = 3913$ km s^{-1} and 3896 km s^{-1}, respectively, with a projected distance of 300 kpc as the only nearby neighbors. For a relative peculiar velocity of 100 km s^{-1}, typical of a small galaxy group, any interaction with the companions would have occurred more than 3 Gyr in the past. Similarly nearby galaxies, including the companions, are not detected in H I 21 cm line emission by the ALFALFA survey (Haynes et al. 2018). Zw 049.057 may be an example of a galaxy that became isolated in its local environment through a merger with its neighbor, the isolation by annexation effect described by Fulmer et al. (2017).

3.3. Color Maps

We used the HST images to make color maps of Zw 049.057 shown in Figure 3. These maps are especially important in revealing the extensive presence of complex dust absorption in the middle of Zw 049.057. The F336W image has low signal-to-noise, and we therefore could not reliably produce a color map that avoided severe detection biases. The color F555W to F125W near-infrared (NIR) image is presented in terms of the

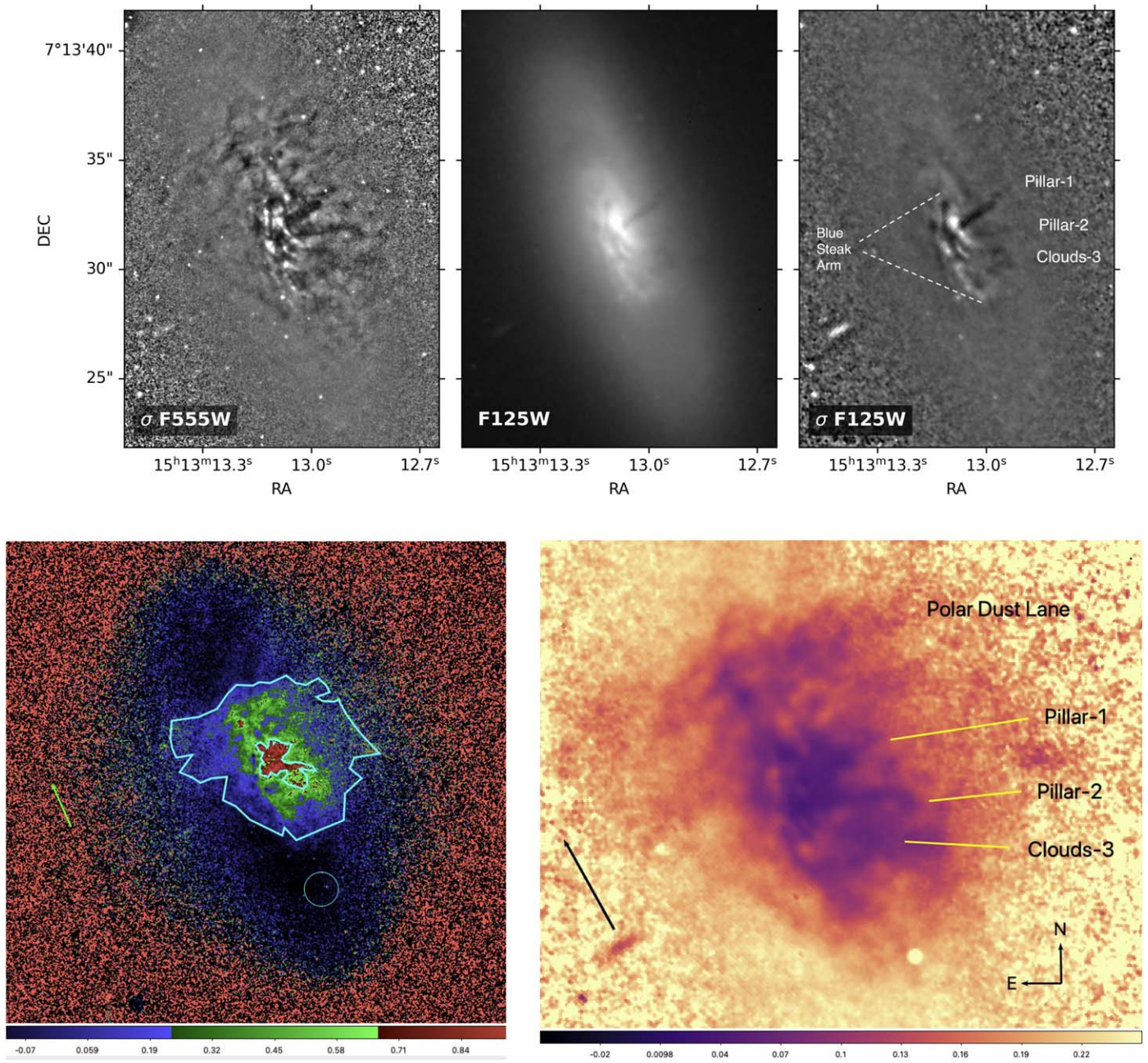

Figure 3. Top panel: large-scale dust absorption structures in Zw 049.057 are shown in our HST WFC3/UVIS F555W and smoothed, background subtracted (σ) images in the F125W filter. Major features are marked; see the text for details. The pair of dust pillars that make up the Zw 0049.057 dust "*V*" are present in our HST F125W image and at longer wavelengths, as shown by Scoville et al. (2000). Pillar-1 stands out in the F125W image, which is consistent with its inferred high optical depth. Pillar-2 to the south is narrower and less pronounced. The asymmetric "blue streak" arm is labeled. Bottom-left panel: the distribution of the observed color $(V-I)_{\rm STMAG} = m({\rm F555W})_{\rm ST} - m({\rm 814W})_{\rm ST}$ shows the central reddening due to the polar ring and extraplanar interstellar matter. Deeper inner dust obscuration is associated with the pillars and outflows on the west side of the galaxy. The outer contour defines the "central region" in Section 4.3 where we measured the average diffuse dust absorption. The inner contour outlines the more heavily obscured region that was replaced by the surroundings for the diffuse region opacity measurement. The color map is at the original pixel scale smoothed by a. $\sigma = 1$ pixel Gaussian. The circle shows an example of a disk region color measurement of $(V-I)_{\rm STMAG} = -0.16 \pm 0.07$, while the deepest absorption around the nucleus has a color of $(V-I)_{\rm STMAG} = $ 0.9. Bottom-right panel: the ratio of the F555W to F125W images in the observed $e^{-1}\,s^{-1}$ matched to the point-spread function of the F125W data and smoothed with a $\sigma = 1$ pixel Gaussian to show regions with a range in optical dust optical depths. Major feature are labeled. The arrow has a length of $3\farcs5$ in both images. A background galaxy is located below the arrow.

ratio of observed count rates where the F555W data were rebinned and convolved to match the pixel scale and approximate point-spread resolution of the F125W image. The central colors of Zw 049.057 are driven by dust absorption. We discuss the properties of the dust in Section 4 below.

The F336W image in Figure 1 displays combined effects of high levels of dust opacity and intense star formation. This complexity is illustrated by the properties of the head of the "blue streak" arm located at J2000 15:15:13.14+07:13:32.6 that is clearly present in the F336W images and also present at longer wavelengths (see Figure 5). We photometered the knot at the northern head of this feature using a $0\farcs13$ radius aperture giving $m_{555,{\rm STMAG}} = 21.7$, $M_{555} \approx -12$ m and $(U-V)_{\rm STMAG,obs} = 0.8$ or close to the color of the Sun. Even this UV-bright region is significantly reddened, but the quantitative obscuration level is difficult to assess because the F555W

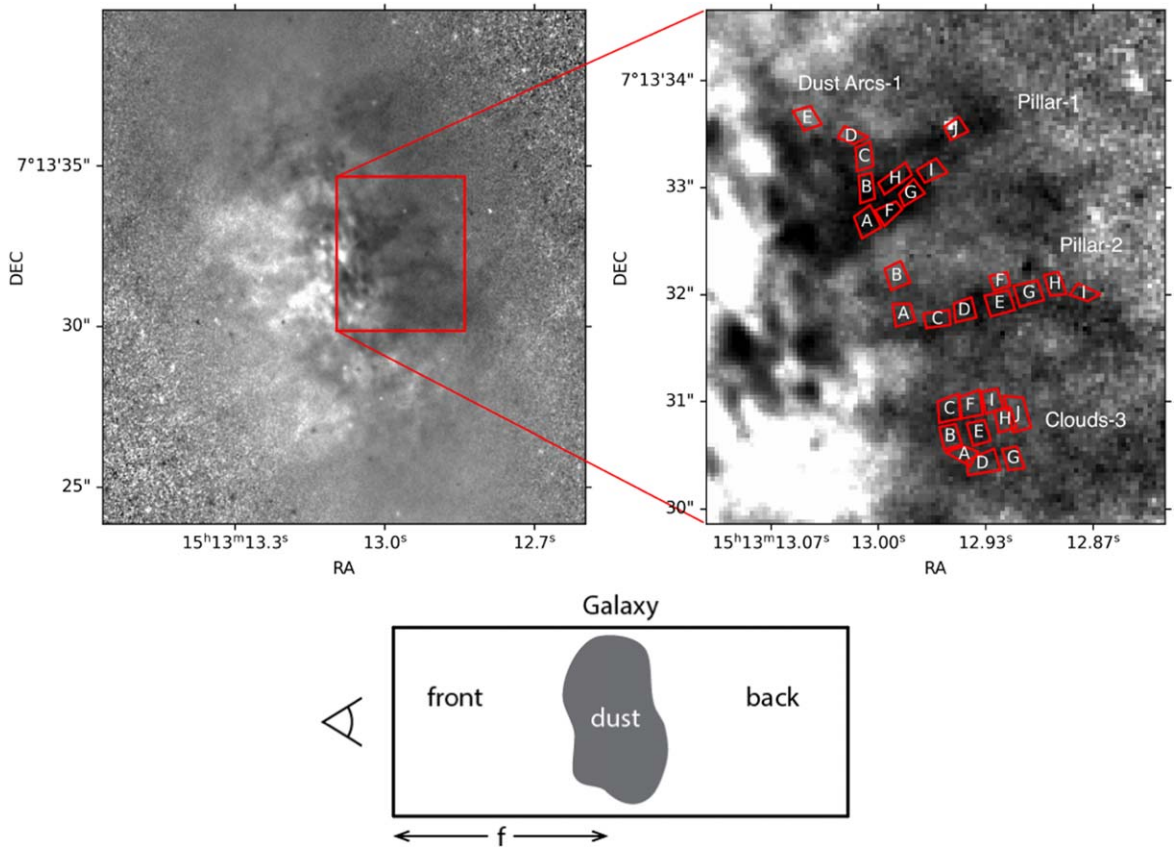

Figure 4. Upper-left panel: the Zw 049.057 F555W image divided by its mirror image along the major axis to distinguish the discreet dust absorption features. Upper-right panel: map of the regions of interest. Pillar-1 is the top grouping, Pillar-2 is in the middle, and Cloud-3 is at the bottom of the image. The boxes labeled with letters define the regions where photometric results are listed in Table 3. Lower-center panel: schematic model of an idealized pillar embedded in a galaxy with constant stellar volume emissivity. Here, f denotes the fraction of the normalized length of the "galaxy" (i.e., $f = 1$ refers to the entire column through the galaxy) to where the uniform opacity cloud is located. This basic embedded cloud model assumes that the width of the dust cloud is small compared to the length of the stellar region. A dark cloud at the surface would be at $f = 0$, and the diagram shows a dark cloud at $f = 1/2$.

image includes a larger background contribution from the surroundings than the F336W image. The measured $(U - V)_{\rm STMAG,obs}$ therefore is an upper limit to the intrinsic color of this region.

The disk beyond the central heavily obscured zone has a roughly constant observed color of $(V - I)_{\rm STMAG} = -0.16$ or $((V - I)_{\rm Vega} \approx 1.1)$ in the bluer and therefore less extincted regions in the main stellar disk. We attempted to model the stellar population in a relatively blue patch of the main disk using GALEV (Kotulla et al. 2010) with photometric data from all of the bands other than the low-quality F336W data. The resulting models spanned a considerable range from a moderately young population with modest dust extinction to a multi-Gyr population with lower extinction. Thus, if the main disk comparison regions are relatively dust free, then the disk contains old stellar populations. A full assessment of the stellar composition of the Zw 049.057 disk will need to await the analysis of our MUSE spectroscopic data (C. Wethers et al. 2024, in preparation).

4. Interstellar Obscuration

4.1. The Dust Absorption Structures

The variety of dust features on large scales is shown in Figure 3. The dust features in Zw 049.057 can be classified into several categories (see Figures 1 and 3 for labels) as follows:

1. A complex of moderate opacity dust covers most of the central regions of Zw 049.057 with a geometry that is indicative of extraplanar material.
2. Dust bands that are slightly convex inward crossing north and south of the galaxy center are polar ring signatures.
3. Dust structures within inner the disk are concentrated within a radius of roughly 1 kpc and have curved shapes roughly following the elliptical pattern of the disk isophotes.
4. Multiple dust features structures are observed to extend from the star-forming inner disk. A prominent example is the Clouds-3 complex spanning the south–southwest of the galaxy center (see Figures 3 and 4 and Section 7.1).
5. Clearly defined linear dust features, Pillars-1 and -2, discovered by Scoville et al. (2000), stand out due to their high opacities and are discussed in Section 4.5. The pillars converge in the area of the nucleus.
6. Faint, approximately linear dust lanes are primarily observed in the F555W on the east side of Zw 049.057 extending outward from the star-forming disk toward a projected point in the eastern halo (see Figure 3). The origins of these features are not clear.

A full accounting of the properties of dust absorption would take into account the physical natures of radiation fields, dust scattering, the geometry of the system, and the physical properties of the dust (see Calzetti 2001; Gordon 2021;

Popescu 2021, for reviews), information that we do not have. Our objective therefore is to apply simple pure absorption models to make initial estimates of dust opacities and associated gas masses. In the sections that follow, we present our analysis of the major dust features within Zw 049.057.

4.2. Dust Properties

The difficulties associated with measuring dust optical depths and deriving approximate gas masses from dust obscuration levels are well known (e.g., Calzetti 1997; Kylafis & Xilouris 2005; White et al. 2000; Natale et al. 2014; Calzetti et al. 2021; Keel et al. 2023). If the dust lies outside of the stellar system, then the foreground dust screen (*fg*) approximation for purely absorption opacity can be used. In the foreground screen case, an absorber with optical depth τ_{fg} is in front of the luminosity sources giving $I/I(0) = e^{-\tau_{fg}}$. This model yields a lower bound to the dust absorption optical depth for cases where the dust lies within the stellar bodies of galaxies. For example, the basic equation for radiative transfer shows that in an optically thick system with a constant spatial distribution of opacity and luminosity density, $I/I_0 \rightarrow S$ where S is the source function, while the foreground screen predicts $I/I_0 \rightarrow 0$. Ignoring scattering and unresolved spatial variations in optical depths along the observed sight lines also leads to underestimates of dust opacities. Our measurements of dust optical depths derived from foreground screen models therefore yield lower limits to the true dust optical depths.

4.3. Diffuse Dust Absorption

The spatial structure of diffuse dust across the center of Zw 049.057 indicates that this material likely lies in a three-dimensional structure that extends above the plane of the stellar disk and includes the northern polar dust lane. This is an area that is dominated by feedback from the galaxy's center and polar material. Therefore, measurements of the mass of interstellar matter in this region provide information on the scale of reservoirs associated with out-of-plane gas flows.

We selected the central dust component selected based on reddening levels in the color map shown in Figure 3 that include the selection boundaries. Two regions in the main disk of Zw 049.057 provided an estimate of the unreddened $(V - I)_{\rm STMAG} = -0.16 \pm 0.07$ for the unreddened color of ZW 049.057. The calculated value of the optical τ_{fg} for a foreground dust screen came from our map of the $(V-I)_{\rm STMAG}$ in Figure 3. We used the standard relationship $m(\mathrm{obs})_\lambda = m(0)_\lambda + A_\lambda$ where the optical depth is $\tau_\lambda = 1.087\ A_\lambda$ and an extinction law $\tau_V = \tau_\lambda(\lambda[\mathrm{nm}]/555)^{-x}$ with $x = 1.3$ (Keel et al. 2023) to find the extinction and convert color excesses into the obscuration levels and optical depths. This process assumes the stellar populations in the main disk are typical of the galaxy as a whole. Therefore, we would underestimate the extinction and optical depths in any regions with bluer colors than those of the main disk. In estimating the central reddening, we removed the innermost highly obscured central region of Zw 049.057 from consideration and replaced the obscuration in this varied zone with the mean reddening from the surroundings. Also, the central region is complex with some dust likely to be embedded or have variations in optical depths, which also leads to underestimates of optical depths. This procedure yielded a conservative $\tau_{V,fg} \geqslant 0.8$ for the central zone of Zw 049.057.

Adopting a Galactic relationship of $N_{\rm H} = 1.9 \times 10^{21}$ H-atoms cm$^{-2} A_V$, $\tau_V = 1.087 A_V$ and a helium mass fraction of 0.27 (Draine 2011), the foreground screen model gave $M_{\rm gas,out} \geqslant 10^8\ M_\odot$ and $\overline{N_{\rm H}} \geqslant 1.4 \times 10^{21}$ atoms cm^{-2} for the extraplanar gas seen in absorption across the central 8×10^6 pc^2 of Zw 049.057 (see also Table 3). Since Zw 049.057 is likely to have a symmetric structure, the total mass of diffuse gas that accounts for the unseen hemisphere is twice our observed value, or $M(\mathrm{gas})_{\rm diffuse} \geqslant 2 \times 10^8\ M_\odot$.

H I 21 cm absorption measurements by Mirabel & Sanders (1988) give a column density of $N_{\rm H} = 6.6 \times 10^{21} (T_s/100\ \mathrm{K})$ where T_s is the H I spin temperature. The agreement between the H I data and dust absorption measurements is reasonable given the considerable uncertainties, including the probability that the H I absorption is observed against the compact nuclear radio source where the ISM is likely to be densest. Therefore, we adopt $M_{\rm gas,extraplanar} \simeq 2 \times 10^8\ M_\odot$ for the important spatially extended central gas reservoir that equals ≈10% of the molecular gas mass in Zw 049.057 (Herrero-Illana et al. 2019). Since most of the dusty gas is observed at projected heights of about 1 kpc, we do not find clear evidence for an escaping galactic wind. Extraplanar gas is likely to be in a dynamic state with the mass balance set by the competition between injection from the galaxy center and remnant merger material in polar orbits versus loss of gas as dissipation allows material to settle back to the disk.

4.4. Embedded Slab Dust Pillar Absorption Models

The linear dust "pillars" that make up the dust "*V*" in Zw 049.057 are sufficiently well defined to be treated as discreet features. For simplicity in calculating optical depths and other parameters, we empirically modeled the pillars as rectangular solid prisms of dusty material embedded within a uniform stellar medium. Consistent with this model, we selected polygonal subregions to pick out the absorption peaks, and analyzed dust opacities via a simplified embedded cloud dust model. Taking advantage of the low extinction above the disk in the northwest and the system's relatively high degree of symmetry, we made an image of the galaxy that is flipped around the disk's major axis. Dividing the galaxy by its flipped image provides an estimate of the galaxy background and the levels of obscuration in the dusty southwestern regions (Figure 4) relative to the northeast side. In a manner similar to that adopted by White et al. (2000), we used this image to estimate the dust transmission levels and thus opacities in the labeled regions in the F555W and F814W filters from the flipped WFC3 HST images in Figure 4. If the east side of Zw 049.057 is somewhat obscured, then this approach underestimates the opacity of the pillars. As can be seen in Figure 4, the dust dark nebulae above and to the west of the central disk plane are complex but reasonably well defined. However, the dust structure in the central star-forming disk is too confused for the flipped background method to be useful.

The presence of physically discreet dust absorption structures embedded within the stellar body of a system complicates the determination of dust opacities from measurements of the light transmission. For example, an optically thick cloud near the far side of an otherwise transparent stellar light distribution would have low contrast, leading to an apparently high transmission; the foreground dust screen model would measure this as a region with low opacity. We largely overcame this problem by taking advantage of the variations in opacity with

Table 3
Obscuration and Gas Masses in Zw 049.057 Extraplanar Absorption Features

Region	Adopted τ_V	Area (arcsec^2)	Area (pc^2)	$N_{\rm H}$ (cm^{-2})	$n_{\rm H}$ (cm^{-3})	Estimated $M_{\rm gas}/M_\odot$
Central Region	0.8	97	8×10^6	1.4×10^{21}		10^8
Pillar-1:						
1A	1.9 ± 0.2	0.042	3500	3.1×10^{21}	17	1.2×10^5
1B	1.8 ± 0.2	0.034	2800	1.7×10^{21}	10	5.3×10^4
1F	$\geqslant 2$	0.040	3300	2.2×10^{21}	13	$\geqslant 8 \times 10^4$
1G	2.1 ± 0.3	0.028	2300	1.7×10^{21}	11	4.3×10^4
1H	1.3 ± 0.2	0.042	3500	2.2×10^{21}	12	8.4×10^4
1I	1.0 ± 0.1	0.030	2500	1.9×10^{21}	12	5.0×10^4
1J	0.8 ± 0.1	0.028	2300	1.4×10^{21}	9	3.5×10^4
Sum 1A-J						5×10^5
Pillar-1 total	1.7:	0.320	2.6×10^4	2.9×10^{21}		$\geqslant 8 \times 10^5$
Pillar-2-mean:						
Sum 2A-2I	1.1 ± 0.1	0.25	2.0×10^6	1.9×10^{21}	$\sim$10	4×10^5
Clouds-3:						
3A	2:	0.029	2400	4×10^{21}		1.0×10^5
3B	2.0 ± 0.3	0.034	2700	3.4×10^{21}		1.0×10^5
3E	1.4 ± 0.2	0.035	2900	2.4×10^{21}		7.5×10^4
3F	2:	0.043	3500	4×10^{21}		1.5×10^5
3G	2.0 ± 0.3	0.030	2500	3.4×10^{21}		9.3×10^4
3H	>2	0.032	2500	$>4 \times 10^{21}$		$> 1 \times 10^5$
Sum 3A-H						$> 5 \times 10^5$
Dust Arc Examples:						
1C	1.6 ± 0.1	0.030	2400	2.7×10^{21}		8.4×10^4
1D	1.5 ± 0.1	0.022	1800	2.6×10^{21}		5.3×10^4
1E	2:	0.034	2800	1.7×10^{21}		1×10^5

Note. Regions and the lettered subregions are defined in Figure 4. Opacities are based on the embedded screen model for Pillar-1, Clouds-3, and Dust Arcs. A foreground screen model was applied to Pillar-2. See the text for details of the approximations used to derive optical depths. As discussed in the text, optical depths are likely to be lower limits, especially for Pillar-1. The "Pillar-1 total" entry is from a rectangular region encompassing the main pillar. Gas masses are derived using a Galactic conversion factor from dust opacities to gas columns, as discussed in Section 4.3. The gas volume densities $n_{\rm H}$ are derived for Pillar-1 and Pillar-2 assuming each subregion is rectangular with a depth equal to the $\sqrt{\rm area}$.

wavelength. A high dust opacity cloud, even if deeply buried within the stellar body, will remain opaque to long wavelengths, and such features can be found from their lack of variation in intensity with wavelength. Gallagher & Hunter (1981), for example, applied this technique to identify molecular clouds in the dwarf galaxy NGC 185.

We approximated this situation with a simple discreet cloud model shown in Figure 4. The model has three unknowns: the fractional location f of the cloud within the stellar system where $f = 0$ on the front surface and $f \leqslant 1$, the visual optical depth of the cloud τ_V, and the extinction law that gives $\tau_{\rm lambda}/\tau_V$. If we assumed a standard extinction law, which is appropriate for the diffuse absorption and applies in most other dusty early-type galaxies (Finkelman et al. 2012, and references therein), then we could solve for f and τ_V from observations at two wavelengths: $I_{\lambda,\rm obs}/I_{\lambda,0} = f + (1-f)e^{-\tau_\lambda}$.

The linear sizes of the sampling regions in the pillars are $\sim$40–60 pc. Although the dust structures within the pillars are not well resolved, both pillars have a thin higher opacity component that appears to be surrounded by less opaque material. If an unresolved mix of dust optical depths exists, then our assumption of uniform opacity under-weights the more opaque regions, and our τ_V are lower limits (e.g., Városi & Dwek 1999). An additional issue arises for locations where we estimate $\tau_V > 2$. At these optical depths, the intensity ratios are $<$0.13, and our measurement uncertainties based on the uniformity of the background area $\pm$ 0.07 are too large to reliably measure such low ratios. The high-density parts of the filaments are at the reliability limits of our data and require an analysis going beyond simple models. Since our methods for deriving τ_V led to underestimates of optical depths, we once again obtained lower-bound estimates of gas masses.

4.5. Properties of the Dusty Polar Outflow Features

4.5.1. Dusty Pillar-1

The distinctive dusty Pillar-1 in Figure 4 is oriented toward a position angle on the sky of $303 \pm 2°$ as measured from the galaxy center. Since the major axis position angle is 19°, Pillar-1 is offset by $14° \pm 3°$ from the minor axis of the main disk. Pillar-1 has a maximum width of 110 pc near its base in the F555W image and narrows to 60 pc near the top of its coherent main structure. The width of Pillar-1 is not sharply defined since the opacity declines toward its northern side, away from the narrow, denser dust spine on the southern edge that has a width of $\leqslant 0\farcs1$ (29 pc). The color map in Figure 5 shows that the spine of Pillar-1, even though clearly in strong absorption at NIR wavelengths (see Figure 5), remarkably, does not display highly reddened colors. The projected length of Pillar-1 is 600 pc to the top of the linear main structure, and it extends in a less-organized way to near 750 pc. If Pillar-1 is orthogonal to the disk, then its deprojected length is about 800 pc. Pillar-1 lies along the center of the minor axis L-band radio emitting region discussed by Falstad et al. (2018), which will be investigated in further detail by Lankhaar et al. (2024). The dust distribution along the length of Pillar-1 is not uniform, and includes a detached dark cloud beyond the termination of the main pillar (Pillar-1, Subregion-J of Figure 4). Our

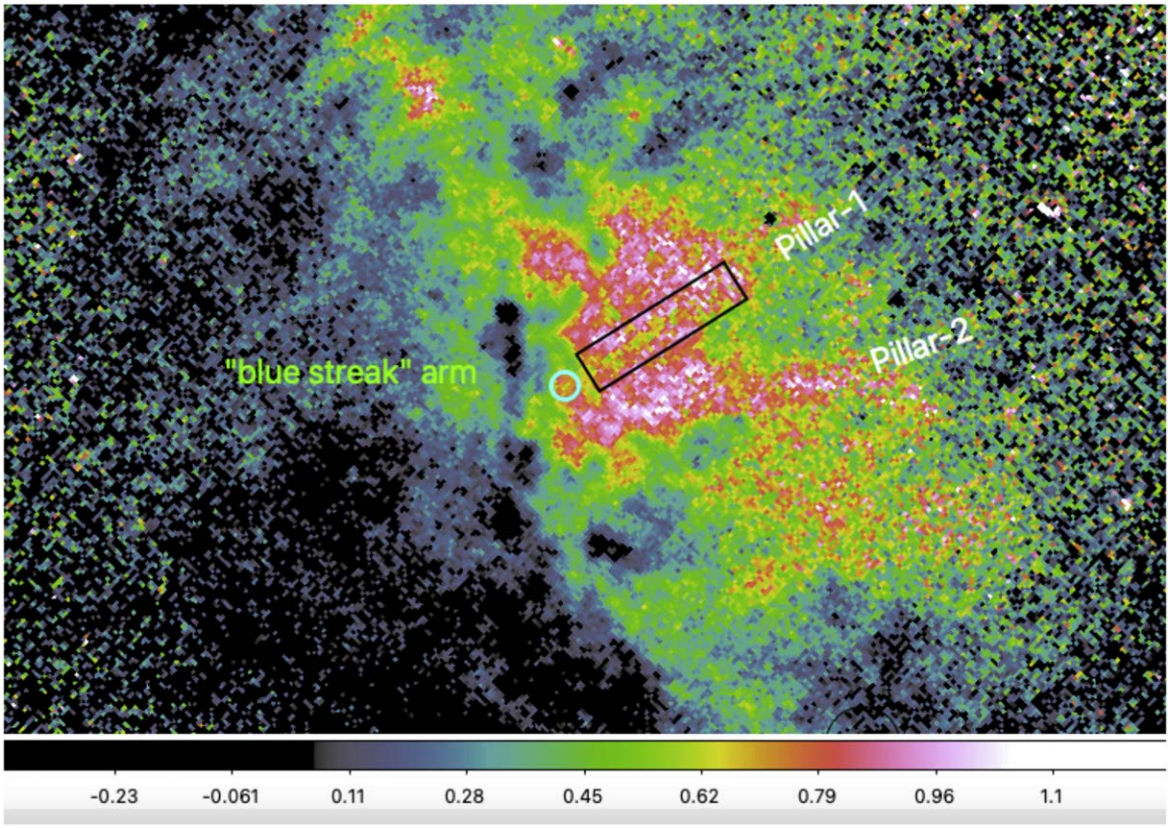

Figure 5. The central region of Zw 049.057 is shown in a full-resolution $(V-I)_{\rm STMAG}$ image with north and east to the left. The location of Pillar-1 is marked by a cyan rectangle. Only the north edge of Pillar-1 is delimited by reddening, while the clumpy Pillar-2 can be traced by its red colors. The color at the location of the Pillar-1 spine is close to that of the surroundings, indicating a high optical depth that limits the transmission of reddened light. The "blue streak" arm is also evident, with the bright northern knot at its head. The $0\farcs15$ circle shows the location of the CON as determined by radio continuum observations.

measurements of transmissions along Pillar-1 focus on the local absorption peaks.

Figure 5 shows the $(V-I)_{\rm STMAG,Obs}$ color map for the center of Zw 049.057. While the northern edge of Pillar-1 shows the expected reddened colors, its core has the color of the less-reddened background. Evidently, Pillar-1 is optically thick in the HST V and I bands so that it blocks most of the background light, leaving only the less-obscured light from the foreground. Pillar-1 fits with the simple model presented in the lower panel of Figure 4 where the embedded cloud is optically thick. By analogy, the lack of the reddening along the Pillar-1 core suggests that it is not in the foreground of our sightline. Therefore, we estimated the obscuration along Pillar-1 using the simple embedded cloud obscuration model.

The results of this exercise gave a fractional depth within the luminous medium $f\approx 0.2$–0.3 and $\tau_V \approx 1$–2 for Pillar-1. Table 3 lists the resulting optical depths, gas mass estimates, and mean gas densities for the main clumps along Pillar 1. This analysis yielded $M_{\rm Pillar1,gas} \gtrsim 8\times10^5\ M_\odot$ for the region projected above the disk of Zw 049.057. Due to our the neglected scattered/reflected light in our simple slab model and insensitivity to the optically thick spine and small-scale substructures, we likely substantially underestimated the mass of gas in Pillar-1. Even so, we found the visually striking Pillar-1 to only have $\gtrsim$0.5% of the $\sim2\times10^8\ M_\odot$ gas mass of the CON (see Section 6), and $\gtrsim$1% of the extraplanar gas. Given the symmetry of the apparently associated L-band radio extension about the center of Zw 049.057 and considerable level of uncertainties, we adopted a total mass in both sides of Pillar-1 of $\gtrsim 2\times10^6\ M_\odot$.

Pillar 1 appears to be spatially connected to the nuclear regions and likely to the CON in Zw 049.057 (Scoville et al. 2000). If Pillar-1 represents a collimated outflow, then we can estimate a minimum lifetime of $t_{\rm fil1} \approx 3\times10^6 (L_{\rm 800pc}/V_{\rm 300\text{-}outflow})$ yr. The outflow velocity of 300 km s^{-1} is chosen to be in a regime where matter could escape and remain collimated from the nuclear region. If Pillar 1 is an outflow feature, it can be produced in a short time.

Alternatively, Pillar-1 could be a part of an approximately conical wall resulting from the fast nuclear outflow seen by Falstad et al. (2019). The pattern of dust reddening in Figure 5 could be due to a dusty outflow with an opening angle of $\approx$30°–40°. The lifetime of a cone wall would be determined by the evolutionary timescale of the outflow, which can be considerably longer than the linear flow time. However, if the pillar is an outflow cone wall, then it is surprising that the structure aligns with a radio continuum plume (Falstad et al. 2018; Lankhaar et al. 2024). A linear shape well above the main disk also is unexpected for an outflow cone, since expansion of the outflow will increase as the surrounding gas pressure drops, allowing the outflow to expand horizontally and break the linear cone walls (e.g., Tenorio-Tagle & Muñoz-Tuñón 1998). Even so, it is likely that a variety of gas outflows from the CON are largely responsible for the pillars and other complex dust structures above the center of Zw 049.057.

4.5.2. Dusty Pillar-2

Pillar-2 has a longer projected length (≈900 pc) and is narrower in the F555W image (≈50 pc) than the more visible Pillar-1. Located at position angle 277° ± 3°, it emerges close to the disk's minor axis and is offset by ≈26° from Pillar 1. Unlike Pillar 1, the presence of Pillar-2 is clear in color maps where it is bounded by a ridge of obscuration and shows reddened colors that are constant along its length to within 0.2 mag. Pillar-2 likely is located in the foreground of our line of sight with only a modest optical depth. Therefore, we utilized the foreground screen model with our adopted power-law opacity representation that we applied to the measured regions to derive the average optical depths and associated quantities in Table 3. Pillar-2 has a total gas mass of $\gtrsim 6 \times 10^5\ M_\odot$. The dust clouds are more clearly clumped along Pillar-2 than in Pillar-1 with a spacing of ≈0.″4 (100 pc). These opacity peaks could be due to internal instabilities in the flow or time variations in the mass-loss rate that would take place on 100 kyr timescales.

4.5.3. The Two Pillars of Zw 049.057

Both of the Zw 049.057 pillars originate from near the center of the galaxy and have substantial dust optical depths, indicating that they mainly consist of molecular gas (see Section 4.5.3). Production of both pillars by a single collimated outflow that changes direction over time, as seen in the NGC 1377 molecular jet (Aalto et al. 2016, 2020), would be difficult to achieve. A discreet jump in the projected angle of 23° plus an additional offset due to the variation in the location of the two pillars along our line of sight would require large changes in the outflow direction. Furthermore, since both pillars have continuous structures, switches in outflow direction would need to occur extremely quickly, in much less than a flow time. In an additional complication, Pillar-2 crosses the main disk of Zw 049.057 about 0.″5 (150 pc) to the south of the location of the CON. If Pillar-2 originates as a collimated structure in the CON, it would need to change direction soon after being launched to avoid connecting to the CON when observed in projection.

Alternatively, Pillar-2 could be associated with a collimated outflow from a second nucleus or a product of a wall compressed by the fast molecular outflow along the major axis that is observed close to the nucleus (see Lankhaar et al. 2024). We discuss these possibilities in Section 7. Due to these uncertainties about the nature of Pillar-2, we do not include the mass of a hidden hemisphere Pillar-2 in our mass outflow estimates.

4.5.4. Extraplanar Dark Clouds and Arcs

Properties of a sample of extraplanar dark clouds in Clouds-3 of Figure 4 and the Dust Arcs (labeled in Figures 1 and 4) are included in Table 3. These features are relatively opaque and therefore likely to be massive. Extraplanar dust in the Clouds-3 region is dominated by a roughly circular group of clouds located about 500 pc above the disk. Our analysis based on the embedded absorbing cloud model indicated that the outer Dust Arcs clumps C, D, I, and J have lower opacity and are likely to be in the foreground. As shown in Table 3, the core of the Cloud-3 complex is optically thick, and our model suggests it is embedded at approximately the same distance within the stellar distribution of Zw 049.057 as Pillar-1. The Cloud-3 structure could consist of material ejected by the starburst or be a part of a disturbed inner polar gas ring. However, the moderately high optical depths for the Clouds-3 favor a connection to the dense ISM of the starburst disk, as observed in other high-SFR galaxies (e.g., NGC 253 and NGC 891; Sofue et al. 1994; Howk & Savage 1997).

5. SALT Spectra of the Zw 049.057 Disk

We obtained a spectrum along the major axis using SALT to explore the central star-forming disk in Zw 049.057. We limit our discussion here to the spatial distributions and kinematics of the emission lines and the Na D interstellar absorption doublet. Optical spectroscopic properties of Zw 049.057 will be discussed in detail by C. Wethers et al. (2024, in preparation) based on VLT-MUSE integral field spectroscopy.

Red optical spectra near the center of Zw 049.057 show strong nebular emission lines from Hα, [N II], and [S II] (e.g., Martin et al. 1988; Poggianti & Wu 2000); e.g., Sloan Digital Sky Survey (SDSS) spectra from the BOSS spectrograph give an Hα emission-line equivalent width of 47 Å. The 2″ diameter BOSS fiber, however, encompasses only part of the inner, optically bright star-forming disk. Based on the observed Hα equivalent width, the central region of Zw 049.057 could be in a starburst state of intense star formation (see also Poggianti & Wu 2000). The SDSS BOSS spectrum also detects faint [O III] emission that is indicative of ionization leakage from an obscured AGN as observed in the CON galaxy NGC 4418 by Wethers et al. (2024). The presence of an AGN is also supported by the Chandra X-ray detection of an obscured central source (Lehmer et al. 2010), central radio compact radio source (Song et al. 2022), and radio continuum plume (Falstad et al. 2018). Unfortunately, while these measurements detect the AGN, they do not lead to reliable estimates of its luminosity.

Emission in the inner regions of Zw 049.057 is seen in red-region spectra from SALT/RSS and includes spatially extended emission lines of He I, [N II], Hα, and [S II] (see Figure 6). All of the emission lines from the central zone of Zw 049.057 are tilted in wavelength, presenting the classic appearance of a rotating nuclear emission ring. Based on our spectrum, the diameter of the inner star-forming disk is ≈6″ (1.7 kpc), as derived from the length of the linear spectrum that is produced by the rotating ring of emission. The emission-line intensities are reduced in the heavily obscured nuclear region over a diameter of ⩽430 pc based on the estimated seeing and our 1.″5 slit width.

The H II spectra of Zw 049.057 in the Hα region are shown in Figure 7. These data illustrate the velocity shift across the disk and the emergence of faint blue and red emission-line wings near the edge of the inner disk. The Hα emission intensity comfortably exceeds that of [N II] throughout the central star-forming zone, with a typical observed ratio of approximately 2:1. Accounting for underlying Hα stellar absorption would further increase the Hα strength; the Hα-to-[N II] emission-line intensity ratio is typical of stellar ionization. Beyond the central disk, the equivalent widths of the emission lines rapidly decline. For example, the peak equivalent width of [N II] λ line is −15 to −17 Å across the star-forming zone, but drops to less than half of this value at radii 3″ beyond the inner disk. The change in emission intensity relative to the stellar background change is associated with a drift of the emission toward the systemic velocity.

The actively star-forming region in Zw 049.057 is several times larger than the typical galactic central molecular zones

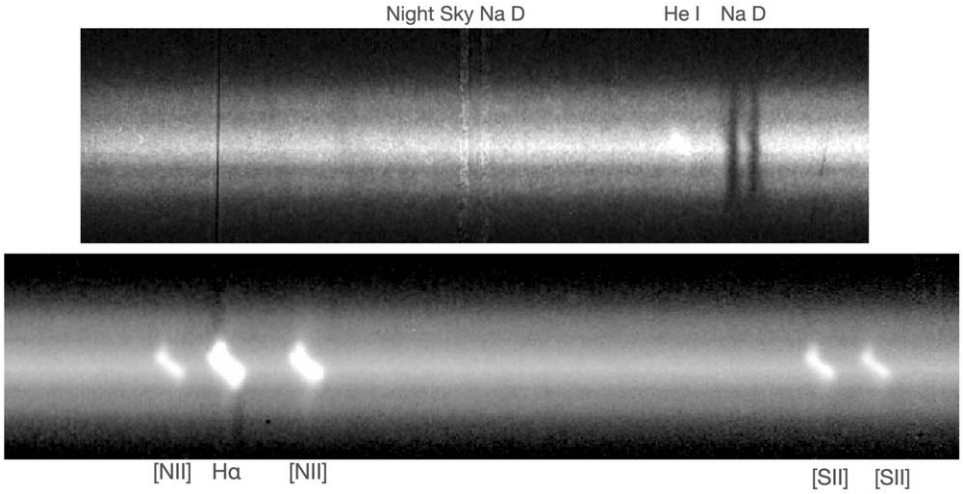

Figure 6. Illustrations of major axis spectra obtained with RSS on SALT. The upper panel shows the linear Na D absorption lines and weak He I λ 5876 Å emission that is inclined due to rotation. Faint stellar absorption lines showing pronounced rotation can be seen blueward of the Na D lines. The spectrum covers a 35″ region along the slit. We plan a full study of the stellar kinematics of Zw 049.057 using integral field spectra from MUSE (C. Wethers et al. 2024, in preparation). The lower panel shows the strong nebular lines from [N II], Hα, and [S II]. These features show rotation in the same sense as stellar absorption Hα lines in the outer disk. Diffuse [N II] emission is visible beyond the central star-forming disk. The spatial width of the lower spectrum also is 35″.

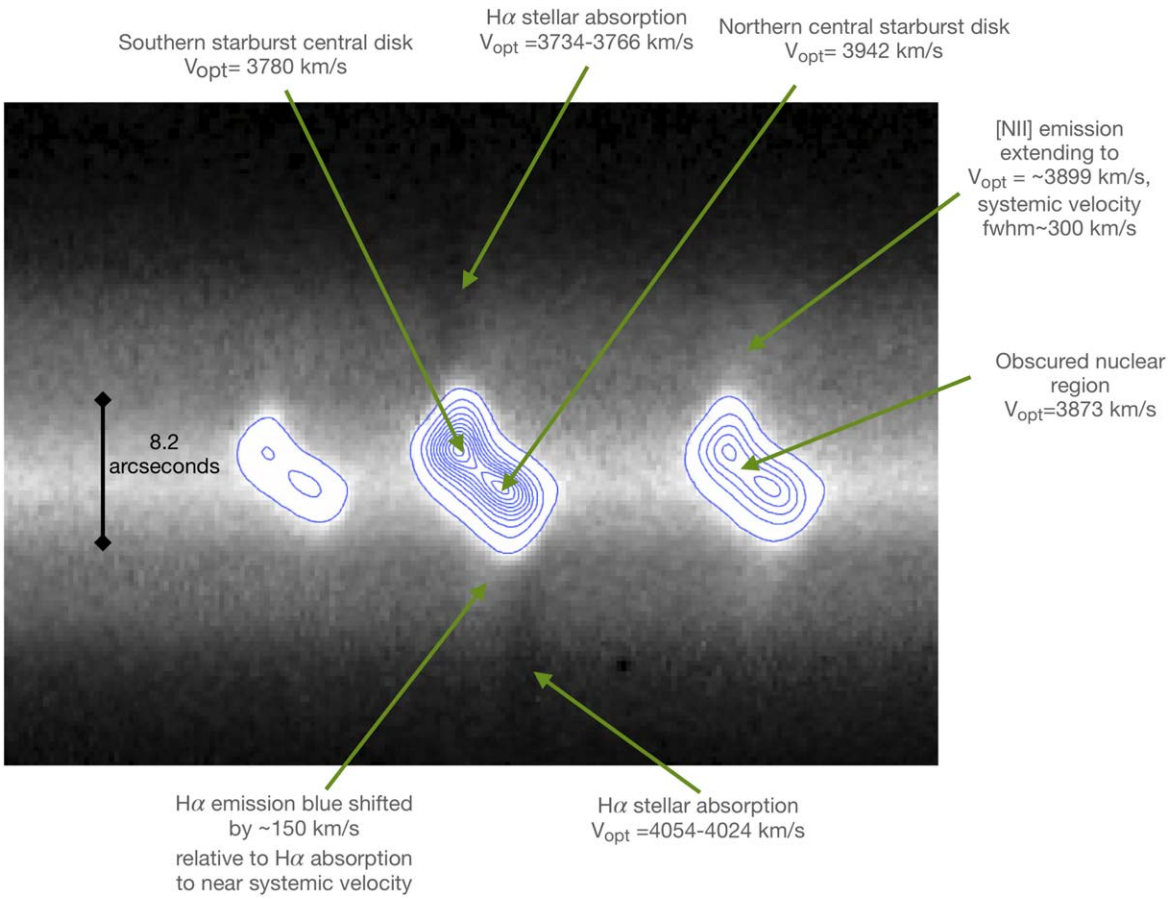

Figure 7. The SALT/RSS spectrum along the major axis of Zw 049.057 shows the presence of three main components of the system: the inner high-SFR disk, Hα absorption from the main disk, and diffuse emission at $R \gtrsim 3''$ from gas near the systemic velocity. Red and blue wings of the [N II] λ 6583 Å line at locations away from the center are due to the superposition of extended faint emission located at the systemic velocity of Zw 049.057. The CON is located within the obscured nuclear region at a scale well below the angular resolution of the spectra.

(CMZs, ∼200–400 pc). The ∼-25 Å equivalent width of Hα emission averaged over the star-forming disk from our spectra indicates active star formation across the inner disk region (see also Poggianti & Wu 2000). Radio data, however, indicate that the SFR beyond the CON-dominated core is not sufficiently high to be a major contributor to the bolometric luminosity and does not clearly qualify as a starburst on the basis of the Hα emission equivalent width, unless dust absorption is reducing

its value by a factor of at least 4 (Bergvall et al. 2016). The *L*-band continuum flux from the NVSS is 53.8 mJy in a 45″ beam (Condon et al. 1998) while Baan et al. (2008) found a flux of 45.7 mJy in a 0.″5 beam. Assuming that the radio source is not variable, we assigned an *L*-band flux of $\lesssim$10 mJy to the star-forming disk beyond the nuclear region. Using the calibration by Kennicutt & Evans (2012), the *L*-band radio measurements gave an SFR of $\lesssim 3\,M_{\odot}$ yr^{-1}, which provides approximately 10% of the $L_{\rm FIR}$ from Zw 049.057, while the optically hidden CON and its surroundings within $r = 100$ pc dominate the luminosity from Zw 049.057.

Figure 7 shows how the kinematics of the H II emission changes exterior to the star-forming disk region and arises from a possibly diffuse ionized gas component centered near the systemic velocity, similar to the situation observed in the CON host galaxy NGC 4418 (Ohyama et al. 2019). Our observed heliocentric velocity near the center of the star-forming disk is $v_{\rm helio} = 3881 \pm 8$ km s^{-1}, while the centroid of the velocity across this disk gives 3888 ± 10 km s^{-1}. The latter measurement is less affected by dust, and we adopt $v({\rm sys})_{\rm helio} = 3888 \pm 10$ km s^{-1}. This is consistent with the velocities observed in molecular lines by Aalto et al. (2015), who assumed $v_{\rm helio} = 3900$ km s^{-1} for their study and the $v_{\rm helio} = 3898$ km s^{-1} found by Mirabel & Sanders (1988) from H I absorption. The absence of emission at the disk rotation velocity in the outer stellar disk beyond the central starburst zone and the lack of young stellar complexes in our F336W image show that the main disk of Zw 049.057 does not support active star formation.

The projected velocity width along the major axis of the star-forming disk and into the main disk is $\Delta v = 150 \pm 10$ km s^{-1}. Correcting for inclination gives a rotation speed of $V_{\rm rot} = 160 \pm 10$ km s^{-1}. This is substantially lower than the $\Delta v_{0.5} = 200$–250 km s^{-1} measured globally from the full CO 1–0 line width at zero intensity by Herrero-Illana et al. (2019), who also found a characteristic double-peaked emission profile from a rotating disk with the intensity peaks at velocities close to the optical measurements. The CO 2–1 rotation curve in the inner 2″ by Falstad et al. (2018) has a peak rotation velocity of $\approx$150 km s^{-1} with turbulent gas and outflowing material contributing to the broader line wings. The molecular line data therefore agree with the our emission-line galactic rotation speed in the disk of Zw 049.057.

We explored emission-line widths using the [N II] λ6583 line because it is not affected by underlying stellar absorption. In the outer part of the star-forming disk, the [N II] FWHMs are measured to reach to nearly 300 km s^{-1}, albeit with modest reliability due to the faintness of the line. Even in the central position, the [N II] line profile is only slightly asymmetric, so the line is well fit by a Gaussian with an FWHM = 180 km s^{-1}. Our exploratory spectra therefore do not show obvious signs of a fast ionized wind from the CON, but we emphasize that this region is heavily dust-obscured, and we are observing along the major axis.

5.1. Kinematics of Interstellar Sodium

Remarkably strong Na D interstellar absorption lines are detected across 20″ (5.7 kpc) of the major axis of Zw 049.057. These lines are relatively narrow, with an FWHM derived from Gaussian fits to the line core of 130 km s^{-1}. The Na D lines are centered at the galaxy's systemic heliocentric radial velocity with $v_{\rm helio} = 3895 \pm 8$ km s^{-1} (see Figure 6). Absorption from Na D does not show the disk rotation but is constant in velocity across the major axis to within 50 km s^{-1}. Therefore it differs from the blueshifted, asymmetric or P-Cygni Na D line profiles observed in cool galactic winds (Martin 2005; Cazzoli et al. 2016; Baron et al. 2020). It also differs from the situation in the CON galaxy NGC 4418 where the Na D absorption contains a rotational signature (Ohyama et al. 2019). The Na D absorptions in Zw 049.057, however, are similar in velocity width and radial velocity to the diffuse [N II] emission detected beyond its starburst disk and the H I absorption studied by Mirabel & Sanders (1988). These features trace a multiphase interstellar gas component that does not display the rotational kinematics of the disk and is not part of a well-defined galactic outflow.

6. The Nuclear Environment

The gas reservoir within the Zw 049.057 CON can be estimated from the model by González-Alfonso & Sakamoto (2019). Assuming a column density of $10^{24.8}$ cm^{-2}, a covering factor for the gas of η steradians, and Galactic H/He, the nuclear reservoir mass is, $M_{\rm nuc,gas} \simeq 3.5 \times 10^8\ (R/R_{\rm 20pc})^2\ (\eta/4\pi)\ M_{\odot}$. For a CON, we expect $(\eta/4\pi) \approx 1$, with some leakage as shown by the presence of [O III] line emission, and adopt $M_{\rm nuc\text{-}gas} = 3.5 \times 10^8\ M_{\odot}$. The CON is well supplied with gas to support star formation, outflows, and/or power an AGN for significant timescales. It is fully obscured until at least millimeter wavelengths, complicating efforts to determine the nature of the power sources within the CON (e.g., Aalto et al. 2015).

HST NICMOS-2 imaging obtained by Scoville et al. (2000) showed the structure of the central star-forming disk, including the region containing the invisible CON, and demonstrated that the CON is located below the highest-opacity dust pillar, a result that we confirm. The central region of the star-forming disk appears to be relatively symmetric without a bar, but the modest resolution in the NIR combined with the presence of dust limit our ability to detect inner stellar substructures. A single, well-defined spiral arm extends to a radius of 3.″5 (1 kpc) along the southern major axis, which is seen as the "blue streak" in the optical images (see Figures 1 and 5). Bright *U*-band knots lying along this arm show that its visibility is enhanced by star formation even though this highly visible arm is substantially obscured by dust. The presence of an asymmetric arm structure fits with the possibility of a relatively recent minor merger where the interloper recently entered into the central region of Zw 049.057 (e.g., Mihos & Hernquist 1994; Laine & Heller 1999; Bournaud et al. 2005).

Using HST images with celestial coordinates updated with data from Gaia, we can locate the hidden CON on our images. Figure 8 shows the nucleus on our F814W image where we adopted a position of 15:13:13.092 + 07:13:31.84 that is the location of the 690 GHz continuum peak found by Falstad et al. (2018). The circle has a radius of 0.″1, which allows for residual positional offsets from the Gaia reference frame. As expected, the position of the CON is close to the lower boundary of Pillar-1 (see Figure 8). However, Pillar-2 is offset from the CON, which is located to the northeast of the projected crossing point between Pillar-1 and Pillar-2. The Pillar crossing point of the two pillars is also near the convergence of two curved disk dust lanes located to the south and west of the center. This region may be part of a multiphase polar wind from the center of Zw 049.057 where a molecular outflow was observed by Falstad et al. (2018; see also Lankhaar et al. 2024). Multiphase winds containing ionized

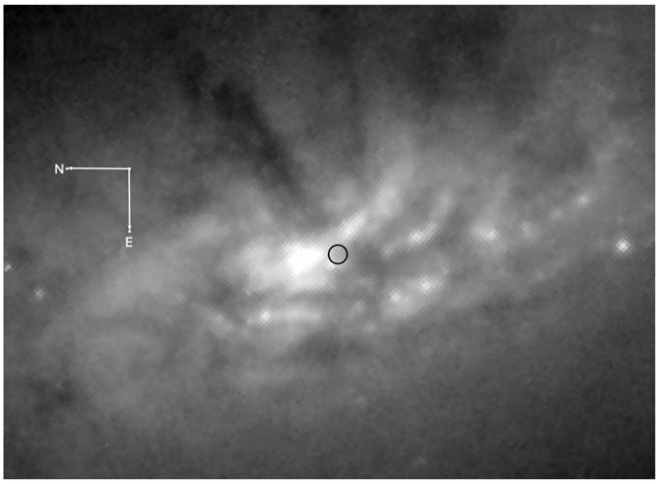

Figure 8. The location of the nucleus is shown with a circle with a radius of 0.″1 on the F814W image of Zw0 49.057. Dust Pillar-1 shows the high-opacity dust spine on its southern edge. Pillar-1 is perpendicular to the bright arc that appears to be in front of the nucleus. This luminous arc is titled with respect to the disk plane of Zw 049.057. Dust Pillars-1 and -2 would be projected to meet ≈1″ east–southeast of the nucleus.The central disk contains a long, spiral arm–like feature (the blue streak in color maps) that extends from the nucleus in the north to the south–southwest. Knots along the arm are star-forming sites, some of which are visible in our F336W image. The compass arms have lengths of 1" each.

and molecular components appear to be a common feature in LIRG CONs (Ohyama et al. 2019; Luo et al. 2022; Wethers et al. 2024).

The CON's position places it near the center of a luminous arclike feature that becomes more pronounced at longer wavelengths. As shown in Figure 8, the luminous arc toward the CON is tilted with respect to the inner disk by approximately 20°. Whether this angular offset is physical or due to varying levels of dust opacity is not clear. The brightness of this arc can be understood if it is an optically thick region that contains active star formation, in which case the surface brightness is determined by the source function, or ratio of stellar emissivity to dust opacity.

7. Discussion

7.1. Zw 049.057: Structure and Interactions

Zw 049.057 is the main member of a small galaxy group. Its only neighbors are two undisturbed dwarfs at projected distances of ∼0.3 Mpc. We classify the stellar galaxy as an S0pec system on the basis of its disklike structure, outer disk colors that are consistent with an older stellar population, and lack of spiral arms in its main stellar disk. The peculiar notation stems from the strong effects of extraplanar dust and presence of the dusty but high-brightness star-forming inner disk. The main stellar disk has a scale length of ≈0.65 kpc, a half-light radius of 0.9 kpc, and, in agreement with previous work, a stellar mass of $1.5 \times 10^{10}\,M_{\odot}$. The most unusual stellar feature in Zw 049.057 is the nearly round outer stellar light distribution that appears at a radius of about 6 kpc. The lack of a large-scale bar in the Zw 049.057 stellar system supports the hypothesis that its CON originated from an external interaction rather than internal secular evolution.

The CMZ and nucleus of Zw 049.057 are highly obscured by dust that is associated with a massive molecular ISM. Our SALT spectra demonstrate that optically visible emission arising from beyond the CON and CMZ is brightest outside of the inner few hundred parsecs, and is in a rotating disk with $V_{\rm rot} = 160\,{\rm km\,s^{-1}}$ that extends to r ≈ 1 kpc. Assuming a spherical mass distribution, the dynamical mass within $r = 1$ kpc is $6 \times 10^{9}\,M_{\odot}$ or ∼40% of the total stellar mass, consistent with the results from the SST photometric stellar mass estimates. This region is relatively gas-rich with $M_{\rm molec}/M_{\rm dyn}$ ∼0.3. Most of the structure within the star-forming disk is due to dust, aside from the single, well-defined "blue streak" arm that from extends the center to a radius of near 1 kpc. We do not detect a nuclear stellar bar, but such a feature could be hidden by dust.

7.1.1. Evidence for a Minor Merger

Our HST images reveal a previously unknown polar ring component of the ISM in Zw 049.057, previously classified as a noninteracting galaxy. The highest-opacity part of the apparently star-free dusty polar ring crosses to the north of the galaxy center, while a second, fainter crossing is present to the south. Polar ring structures are rare and originate from galaxy–galaxy interactions or mergers. Given the absence of nearby companions, the presence of a polar ring demonstrates that the evolution Zw 049.057 was perturbed by a merger (see, e.g., Józsa et al. 2009, for a discussion of similar issues for the "spindle galaxy" NGC 2685). Models show that when a galaxy disk is present, material from a merging companion experiences tidal torques (e.g., Arnaboldi et al. 1993) These lead to twists toward the stellar disk plane and can feed material into the central zones of the galaxy (e.g., Józsa et al. 2009; Sparke et al. 2009). Unfortunately, since the timescale for the disruption of polar rings can be as long as ∼1 Gyr (Mapelli et al. 2015), the presence of a polar ring does not usefully constrain the time span since the merger occurred in Zw 049.057.

A past merger also offers an explanation for the circular outer isophotes in Zw 049.057. An interaction within an intruder can produce rapid angle changes in the orbital plane of disk stars either through warping of preexisting stars or the addition of tidally stripped material from the intruder (Sparke et al. 2009). Color measurements of the outer disk would help to distinguish its origin. Material from a lower-mass intruder is expected to be more metal poor and thus bluer than the colors of the coplanar outer main disk of Zw 049.057, but our data are too shallow to provide this information. The central concentration of dense interstellar matter, "blue streak" inner arm, and possible misalignment of the central region containing the CON also can be understood in the context of a merger. The high degree of overall symmetry of the outer stellar body of Zw 049.057 further suggests that this was a minor merger that did not lead to strong disruption of the stellar disk. As a minor merger, Zw 049.057 fits with general trends observed for dusty early-type galaxies. Most of these systems show evidence for the accretion of dusty gas, frequently from mergers with gas-rich dwarfs onto previously gas deficient early-type galaxies (e.g., Kaviraj et al. 2012; Finkelman et al. 2012; Shabala et al. 2012; Alatalo et al. 2013; Glass et al. 2022). In this case, the intruding galaxy should have entered its final stage, arriving into the center of Zw 049.057, possibly producing the "blue streak" arm. The timescale for this final stage in the merger process is set by dynamical processes and is in the range of tens to hundreds of Myr (Laine & Heller 1999).

Zw 049.057 therefore joins the classic LIRG CON galaxies NGC 4418 (Boettcher et al. 2019) and IC 860 (Luo et al. 2022)

as products of mergers or past interactions. Mergers or interactions that compactify the ISM in galaxies offer a channel to produce dense central gas concentrations that could be favorable for formation of CONs. In this sense, the classic CONs in LIRGs could be considered to be an extension of the more frequent ULIRG CONs that are in merging galaxies. However, not all CONs in LIRGs are necessarily in galaxies that experienced significant recent interactions; e.g., the case of the noninteracting galaxy ESO 320-G030 (González-Alfonso et al. 2021). Furthermore, the LIRG CON hosts fundamentally differ from most of the ULIRGs. Classic LIRG CONs are in early-type galaxies in the late stages of minor mergers versus ongoing mergers between massive galaxies in ULIRGs. The emergence of the CONs in the classic LIRGs appears to be delayed with respect to the peak of the merger activity. Zw 049.057 and the other two classic LIRG CON mergers fit with the pattern for the activation of nuclei during late-phase mergers in early-type galaxies (George 2017; Sazonova et al. 2021; Smercina et al. 2022). The current information therefore places the classic LIRG CONs in the sequence of minor-merger/interaction-induced star formation and nuclear activity that exists broadly among the population of moderate-mass early-type galaxies in the local Universe.

7.2. The Dusty ISM

7.2.1. Central Dust Obscuration

Dust absorption features within and above the central disk are the defining optical features of Zw 049.057. This material with a mass of approximately $2 \times 10^8\,M_\odot$ is likely to be largely in the form of H I and the source of the observed H I 21 cm absorption line. This medium is observed in the optical Na D and diffuse [N II] emission lines that do not show evidence for significant rotational support. The Na D, [N II], and H I absorption lines have modest velocity dispersions of $\sigma = 50-60\,\mathrm{km\,s^{-1}}$ but no significant peculiar velocity offset from the central heliocentric velocity of $3890 \pm 10\,\mathrm{km\,s^{-1}}$ that we find for Zw 049.057. We do not detect an outflowing ionized galactic wind, but our data are limited because the slit position lies along the major axis.

Since the polar ring is seen nearly edge on across the disk, it provides a possible source for the low velocity width neutral gas component. However, since the Na D absorption covers ≈5.7 kpc of the main disk, diffuse gas in the polar ring would need to be more spatially extended than the polar dust lanes that are crossing the disk to produce a low velocity gradient.[14] This H I-rich ISM component appears to be an extraplanar medium supported by turbulence (e.g., Boettcher et al. 2019), a point to be more fully explored once data on the full velocity field of the extraplanar neutral medium become available from the C. Wethers et al. (2024, in preparation) MUSE data. Alternatively, nonrotating gas could be associated with the nearly circular outer stellar distribution that we interpret as a face-on disk component produced by warping during the past interaction. However, in this case, it is not clear how or why the gas would have a high velocity dispersion and retain face-on kinematics when seen in projection against the moderately inclined main stellar disk of Zw 049.057.

[14] An SALT spectrum that we obtained through the center of Zw 049.057 along the minor axis also lacks evidence for rotation in the Na D absorption line, as might be expected if the absorbing gas is in a polar ring.

Even though the diffuse interstellar matter component of Zw 049.057 contains only about 10% of the gas mass, its diffuse structure makes it an effective $\tau_V \sim 0.8$ obscuring screen across the central galaxy. The injection of modest amounts of dusty gas into extended regions around galaxies is an efficient path to ultraviolet obscuration that does not require large amounts of energy or mass. That the diffuse material has low or strongly misaligned angular momentum with respect to the disk is interesting in terms of its potential to feed matter into the CON that requires the collection of substantial masses of low specific angular momentum gas into a radius of $\lesssim$100 pc. Since the medium is turbulent, dissipation is occurring, so the Zw 049.057 extraplanar medium is not likely to be a static structure. The possibility exists that gas with low or misaligned angular momentum falling back onto the disk from the extraplanar diffuse ISM plays a role in fostering inflows that sustain the Zw 049.057 CON.

7.2.2. Dust and the Starburst

Dust clumps are frequently present in the inner disk of Zw 049.057 and dusty structures with a variety of sizes and structures also extend above the star-forming disk. The dense regions in our Clouds-3 location reach heights of ≈500 pc beyond the Zw 049.057 midplane and contain masses of $\sim 1 \times 10^5\,M_\odot$. These dark clouds are likely associated with concentrations of massive stars as is seen in other galaxies with active star formation (e.g., Sofue et al. 1994; Howk & Savage 1997). While lower-opacity connections to the dense clouds reach higher elevations above the disk, it appears that the vertical extent of dusty gas ejected by young stars at $r > 100$ pc is limited. This material is unlikely to be sustained above the disk and is likely to fall back into the disk in cycles driven by the local intensity of star formation. Despite the high gas densities, no evidence for ongoing star formation is found in our HST images of the extraplanar dusty regions.

The low level extensions of dusty gas above the Zw 049.057 starburst, the dust clouds and arcs, combine with the molecular medium in the disk to block most of the light from the starburst. This effect can be seen in Figure 8 where multiple clumps dust clouds and lanes block most of the moderately inclined inner disk. The inner disk contributes to the high opacity of the galaxy, helping to reduce its optical/ultraviolet luminosity and lead to this system being an ultraviolet drop-out with $(U_{\mathrm{F336W,STMAG}} - V_{\mathrm{F555W,STMAG}}) \sim 2$. The presence of the actively star-forming disk is only quantitatively detected via the Hα region emission in Zw 049.057, and even in this case the level of the star-forming activity is difficult to estimate from the optical emission lines due to dust obscuration.

7.3. Dust Pillar Outflows

The pair of dust pillars in Zw 049.057 are direct evidence that the outflow from the nuclear region of Zw 049.057 feeds material out of the disk plane, extending to vertical distances of ≈1 kpc. The Zw 049.057 dust pillars are optically thick into the infrared, and our analysis of their dust optical depths indicates they mainly consist of molecular material. Lower-bound mass estimates for the gas in the two pillars based on simple dust absorption models are $\sim 1 \times 10^6\,M_\odot$ or <1% of the total ISM mass.

The physical nature of the pillars is not yet fully understood. Falstad et al. (2018) and Lankhaar et al. (2024) showed that

C- and *L*-band radio radio continuum emission is present in the direction of Pillar-1, indicating that an outflow is present similar to the types found in other galaxies with gas-rich nuclei (e.g., Alatalo et al. 2014; Luo et al. 2022). The radio continuum flux rises to lower frequencies and is likely to have a significant nonthermal emission component. The radio-molecular jet correlation in Zw 049.057 then suggests an outflow from an AGN that produces a nonthermal radio jet. If the pillars are individual outflows, then they remain remarkably well collimated over their lengths, a situation that is observed with the Atacama Large Millimeter/submillimeter Array by Aalto et al. (2016) and Aalto et al. (2020) in jets emerging from the dusty nucleus of the early-type galaxy NGC 1377. This requires a fast outflow velocity that may be detected by future molecular line observations. In this scenario, the presence of two outflow pillars requires two sources, e.g., possibly the presence of a second nucleus with an associated nuclear outflow or bidirectional outflows from a single nuclear region.

Alternatively, the dust "*V*" extending from the center of Zw 049.057 toward the west could mark walls of interstellar gas compressed by the inner fast molecular wind along the minor axis recently mapped by Lankhaar et al. (2024). If both pillars are part of an outflow cone, then ideally the point of the cone's "*V*" should be at the origin of the outflowing wind. However, the centerline of the "*V*" is slightly offset by ≈5°–10° from the pole of the disk. An extension of the directions of Pillars-1 and -2 meets approximately 0.″5 (150 pc) to the south–southeast of the CON. If a conical structure is present, it does not have a simple symmetric structure. The fast molecular wind observed from the CON in HCN is at PA = 105° and therefore lies between the two dust pillars. However, this region located between the pillars does not show clear signs of extra dust extinction (see Figures 3 and 5). Evidently the fast molecular wind either does not have a substantial dust optical depth or is not present at distances of $\gtrsim$100 pc from the CON where the HST imaging becomes useful. While a model where the pillars are associated with collimated outflows from the nuclear region of ZW 049.057 provides a natural explanation of their unusual structures, the presence of a nuclear molecular outflow along the minor axis of Zw 049.057 producing compressed walls cannot be excluded, especially for Pillar-2.

Assuming the pillars are collimated flows and that symmetry applies such that Pillar-1 emerges on both sides of Zw 049.057, the pillars contain $\gtrsim 2 \times 10^6\,M_\odot$. As discussed in Section 4.5.2 for a collimated outflow, $\dot{M}_{\rm pillar} \simeq M_{\rm pillar}/t_{\rm flow}$ and an outflow velocity of 300 km s^{-1} leads to an estimate of a pillar mass feeding rate of $\dot{M}_{\rm pillar} \gtrsim 2\,M_\odot$ yr^{-1}. This value is a lower bound because we are not sensitive to optically thick regions, such as the spine in Pillar-1, that can carry much of the mass (see Aalto et al. 2020). If the wider opening angle, more diffuse, and faster molecular outflow traced by HCN escapes from the nuclear region, then mass-loss rates from the CON will be considerably higher than those based our analysis of dust optical depths in the pillars.

In Zw 049.057, the termination of the nuclear outflows may not simply result from the velocity of the injected material, e.g., as in a ballistic model. First, the outflows' lengths may reflect timescales during which the nuclear region ejects collimated flows. Second, gas in the diffuse medium or in polar orbits is present above the plane leading to shocks that could disrupt the collimated outflows. This process could provide a mechanism to feed energy into the diffuse neutral medium that would be needed to sustain its dispersion of 50–60 km s^{-1}. It also would offer a process whereby gas from the nucleus returns to the disk where its low specific angular momentum can stimulate inflows to the CON. The relationship between nuclear outflow(s) and the H I-dominated diffuse ISM that covers 6.8×10^6 pc^2 in the center of Zw 049.057 merits further study in the context of galactic level gas recycling (Aalto et al. 2019). If this region is fed by the CON, even an outflow carrying $\dot{M} = 2$–$3\,M_\odot$ yr^{-1} could produce the diffuse extraplanar ISM in ∼50 Myr, provided that the terminated outflows expand to fill a nearly galaxy-wide volume.

The lifetime of the CON in Zw 049.057 depends on how long the nucleus can retain its shroud of dense interstellar matter. The length of Pillar-1 provides a minimum CON lifetime of a few million years. The upper limit on the CON lifetime depends on the still unknown balance over time between gas outflows and inflows. However, CON lifetimes of ∼100 Myr are possible if gas is efficiently recycled between the surrounding ISM and CON (e.g., Gorski et al. 2024). Falstad et al. (2015) and Lankhaar et al. (2024) presented evidence that the required gas inflows may exist for keeping the Zw 049.057 CON fueled for more than an internal gas loss time span. Our observations bear on this issue by showing the possibility of an outflow-fallback recycling mechanism associated with the pillars in Zw 049.057, potentially aided by infall from the past merger and the associated presence of diffuse interstellar matter that has low or strongly misaligned angular momentum.

7.3.1. The Nucleus

The CON, as expected, is hidden from optical view. Its projected location lies within a luminous arc that could be the edge of a CMZ disk. If so, the tilt of the region suggests an offset in angle from the main disk of Zw 049.057 potentially associated with the merger. However, due to the presence of extensive dust absorption in the optical and NIR, this possibility should be confirmed by high angular resolution observations at longer wavelengths. The luminous appearance of this arc shows that it supports star formation, as is observed in other dust arcs in the central disk of Zw 049.057. Even though the compact CON containing an AGN (Song et al. 2022) is completely obscured, its presence in Zw 049.057 is indirectly revealed at optical wavelengths by its connected kiloparsec-scale, highly structured dust pillars in Zw 049.057. The presence of filamentary or collimated outflows from a nuclear region on kiloparsec scales is a signature that can be used to survey for candidate classical CONs in early-type galaxies.

The combination of high power density and dust opacity are key features of CONs. In Zw 049.057, these factors lead to the low ratio of $M_*/L_{\rm IR}$ ≈0.05, suggesting that low $M_*/L_{\rm IR}$ also may be a way to search for current epoch CONs in samples of dust-obscured galaxies. This approach can be especially powerful when combined with mid-IR spectroscopy as discussed by García-Bernete et al. (2022) as well as the more standard molecular spectroscopy (e.g., Falstad et al. 2021). The $M_*/L_{\rm IR}$ selection method, however, may not apply to young star-forming dusty galaxies seen at moderate-to-high redshifts. The discrimination between the contribution from a rapidly star-forming population and a CON is likely to be less well defined in galaxies where dominant young stellar populations drive down the critical stellar M_*/L_{bol} ratio and where compact galaxy sizes facilitate heavy levels of dust obscuration. For

these systems, measurements that are sensitive to line emission from "greenhouse" regions with high submillimeter optical depths and high power densities are required to search for CONs.

7.3.2. The Central Back Hole

The high central molecular mass concentrations in combination with the high power outputs of CONs present a dynamic environment where central SMBH growth is possible. Unfortunately the division of the CON's luminosity between recently formed stars, gravitational potential energy released by infalling gas, and accretion onto an SMBH is not known (Gorski et al. 2023). As an extreme example, if 90% of the luminosity from Zw 049.057 is from black hole accretion, then the SMBH accretion rate would be about $0.06/\eta\, M_{\odot}$ yr^{-1} where η is the SMBH efficiency factor for the conversion of mass into energy. Whether this results in substantial growth depends on the current mass of the central black hole and the lifetime of the CON phase. Presumably the nucleus will exit from the CON phase once its internal gas supply is depleted. An AGN in the Zw 049.057 (e.g., Lehmer et al. 2010; Song et al. 2022) producing $0.9L_{\rm FIR}$ from accretion onto an SMBH might have the potential to sustain itself for 10^8 yr provided that mass loss via winds is very modest. In this optimistic situation, the central SMBH would increase in mass by $\sim 6 \times 10^6\, M_{\odot}$. Issues include the time span over which this level of luminosity can be sustained by the AGN and the ability of the accreting SMBH to operate at sufficiently high luminosity. These factors in turn constrain the amount of mass growth by an SMBH during a CON evolutionary phase.

A complication arises if the central AGN in Zw 049.057 follows the trends observed between the black hole Eddington factor $\lambda_{\rm Edd} = L_{\rm AGN}/L_{\rm Edd,BH}$ and central gas column density found for AGNs by Ricci et al. (2022). Due to the increased opacity of dust, the Eddington limit is reduced and we would expect $\log(\lambda_{\rm Edd}) \lesssim -1.5$. This limit is set by luminosities where radiation pressure from the accreting can readily eject the surrounding dusty gas (e.g., Ricci et al. 2017; Ishibashi et al. 2018; Venanzi et al. 2020). An SMBH producing 90% of the luminosity in Zw 049.057 following this dust radiation pressure constraint needs to have $M_{\rm bh} \sim 10^8\, M_{\odot}$ and so would experience insignificant growth in mass even during a 100 Myr CON evolutionary time span.

This requirement is in tension with the likely SMBH mass. Adopting an upper limit to the bulge mass for Zw 049.057 based on our $M_{\rm dyn} - M_{\rm molec} = 4.5 \times 10^9\, M_{\odot}$, and applying the bulge mass-SMBH mass calibration of Saglia et al. (2016) gives $M_{\rm SMBH} \lesssim 3 \times 10^7\, M_{\odot}$ for Zw 049.057. The more modest mass SMBH that is expected in Zw 049.057, when constrained by radiation pressure limits on $\lambda_{\rm Edd}$, would provide much less than half the $L_{\rm bol}$ in Zw 049.057. Significant black hole mass growth via accretion in Zw 049.057 is most likely for low-mass central black holes with $M \lesssim 10^7\, M_{\odot}$ operating at high $\lambda_{\rm Edd}$ for 100 Myr time spans and avoiding catastrophic radiation-driven dusty gas loss. By analogy with accretion onto massive protostars (e.g., Krumholz et al. 2005; Kuiper & Hosokawa 2018; Gorski et al. 2024), several factors in Zw 049.057 could allow for a high Eddington factor and significant SMBH mass growth without producing excessively rapid gas loss. For example, the dust envelope in the CON is unlikely to be spherical and homogeneous, spatially extended [O III] optical emission is a signature of AGN ionizing radiation escaping through holes in the CON (e.g., Wethers et al. 2024), a substantial molecular wind is observed that carries away momentum, the mass of gas in the CON can help to stabilize the system, and inflowing gas can produce ram pressure (see Aalto et al. 2020; Gorski et al. 2024). Measurements of the mass distributions within the nucleus of Zw 049.057 and other CONs can test the high-mass SMBH CON model and lead to better constraints on the evolutionary connections between CONs and SMBH growth.

7.4. Evolution

7.4.1. CON Formation

Even though minor mergers are associated with CONs, the evolutionary processes that lead to CONs are not understood. We considered the possibility that CONs could preferentially form in galaxies with massive nuclear star clusters and black holes. Alternatively, nucleus–nucleus interactions are known to produce CONs in major merger ULIRGs, and are a natural outcome when both galaxies have nuclei (Downes & Solomon 1998). In minor mergers, the intruder will be a low-mass dwarf galaxy that is less likely to contain nuclei (Matthews & Gallagher 2002; Reines et al. 2013), and when present, nuclei are not normally surrounded by a dense molecular medium. However, the offset dual pillars in Zw 049.057 allow for the possibility that a second nucleus is present and fostering the central concentration of gas around the original, more massive nucleus of Zw 049.057.

In the merger scenario, early-type LIRGs such as Zw 049.057 are caught in a late phase of the merger process with a starburst in progress. Unfortunately, a simple correlation is not seen between merger phase and properties of the CONs in the three classic LIRG CONs NGC 4418, IC 860, and Zw 049.057. Instead variations exist within this small LIRG CON sample between the dominance of the CON relative to its immediate surroundings. For example, NGC 4418 contains a CON but displays a strong post-starburst spectrum beyond its nuclear region (Varenius et al. 2014; Ohyama et al. 2019; Boettcher et al. 2020). Its evolution may be in a different stage and possibly driven by different processes, such as gas accretion from a companion rather than a minor merger (Boettcher et al. 2020). IC 860 has developed a strong outflow and its stellar body to be more highly disturbed than Zw 049.057, suggesting it is in an earlier phase of a merger than Zw 049.057 (e.g., Luo et al. 2022).

These differences might be understood if CONs form rarely during minor mergers, e.g., via an unusual channel such as interactions between dual nuclei, but once present have lifetimes in the 100 Myr range. Under this assumption, CONs can be present throughout late merger/early postmerger stages, similar to the pattern for AGNs to emerge in postburst galaxies (Yesuf et al. 2014; Li et al. 2019). The converse position would be for CONs to frequently form in LIRGs but to be short-lived. In this model, the CON fraction in LIRGs of 10%–20% (Falstad et al. 2021) is proportional to their lifetimes relative to the $\sim$100 Myr LIRG lifetimes (Marcillac et al. 2006; Pereira-Santaella et al. 2015; Cortijo-Ferrero et al. 2017). A CON such as that in Zw 049.057 could readily live for 10–20 Myr after which masses in outflows would naturally lead to the rapid depletion of its cloaking gas. Short-lived CONs would experience limited gas recycling, potentially in combination with star formation, and would not have time to contribute

significantly to accretion-driven mass growth of a central SMBH.

If the limit imposed by radiation pressure must be met to be a CON, then any pre-CON nuclei might also need to be sufficiently massive to overcome rapid gas loss due to radiation pressure as the CON forms. This condition could be achieved by a sufficiently massive black hole with a low $\lambda_{\rm Edd}$ aided by a massive nuclear star cluster. Therefore, the presence of unusually massive galaxy nuclei is a possible factor in the production of luminous CONs through their ability to retain dusty gas while operating at high luminosity.

7.4.2. Timescales

The inner stellar disk is the site of optically detectable star formation in Zw 049.057 (see Section 5 and Poggianti & Wu 2000; Scoville et al. 2000; Alonso-Herrero et al. 2006). Star formation in early-type disk galaxies frequently is concentrated in the inner regions (Rathore et al. 2022), so Zw 049.057 follows the usual pattern. Radio flux measurements show the spatially extended young stellar population has an SFR of about $3\,M_\odot$ yr^{-1} that contributes only about 10% the luminosity of Zw 049.057. The molecular mass of $1.5 \times 10^9\,M_\odot$ yr^{-1} in the inner disk gives a gas exhaustion time of 0.5 Gyr. Zw 049.057 is a marginal starburst if we limit our consideration to the inner star-forming disk well beyond the CON. However, for a normal stellar initial mass function, a total SFR of $24\,M_\odot$ yr^{-1} is required to produce half of the luminosity from Zw 049.057, as, for example, assumed by González-Alfonso & Sakamoto (2019). Since radio data show the bulk of the bolometric luminosity from Zw 049.057 arises from r $\lesssim$ 100 pc, most of the star formation in Zw 049.057 could be within this region that is dominated by the CON. Without a CON, Zw 049.057 would be a normal early-type galaxy with active star formation that would lack the luminosity to be classified as an LIRG.

Unfortunately, the division between power supplied by a central AGN and star formation within the CON cannot yet be disentangled. While the central SMBH cannot absorb a significant fraction of the CON's mass, star formation is an especially important gas sink. For example, a CON region SFR of $20\,M_\odot$ yr^{-1} with a normal stellar initial mass function would exhaust the Zw 049.057 CON's $3.5 \times 10^8\,M_\odot$ gas supply in about 17 Myr. Winds from a rapidly star-forming CON will further reduce its lifetime. Increasing the lifetime of our hypothetical high-luminosity, star-forming CON to 100 Myr would require extremely efficient recycling and involvement of $\geqslant$ 50% of the gas in the galaxy to be processed into stars. This extreme situation would leave a very massive, $\sim 10^9\,M_\odot$ yr^{-1}, postburst stellar population within $r \lesssim 100$ pc. This extreme situation, however, is unlikely for a variety of reasons including issues with angular momentum, although the stellar masses in the centers of compact galaxies such as M32 approach this level (Janz et al. 2016).

Once an early-type LIRG such as Zw 049.057 reaches the post-CON stage, it may show little evidence of having been in a minor merger, and probably would have the stellar properties of a postburst, early-type galaxy. Any remnants of extreme star formation or dense gas associated with the CON would be very centrally concentrated, the H I content is unlikely to be high, and the previously obscured nucleus may emerge as an AGN. If star formation were an important factor in the CON's evolution, the nuclear star cluster and its surroundings would be abnormally massive. In the case where the CON does not support extreme star formation, these properties are consistent with the established trends among postburst early-type systems (e.g., Kannappan 2004; Stark et al. 2013; Sazonova et al. 2021; Smercina et al. 2022). CON LIRGs are one evolutionary channel associated with processes leading to early-type postburst galaxies but in ways where the central SMBH and nuclear star cluster may have experienced a profound and active period of star formation, mass growth, and feedback.

8. Conclusions

Optical and NIR imaging with HST and a major axis Hα region spectrum taken with SALT reveal a variety of interesting features in the CON hosting LIRG Zw 049.057. As one of the nearest examples of a CON, the properties of this system provide new insights into the nature of interactions between a powerful CON and its host galaxy and associated feedback.

1. Our discovery of a polar dust ring demonstrates that Zw 049.057, like several other LIRG CONs, is the product of a minor merger that led to the central concentration of the molecular ISM in the inner kiloparsec of Zw 049.057.
2. Diffuse dust absorption with $\tau_V \approx 0.8$, corresponding to a gas mass of $\gtrsim 2 \times 10^8\,M_\odot$, screens the central $\sim$2 kpc^2 of Zw 049.057 at optical and shorter wavelengths. This complex, turbulent medium has a multiphase structure including ionized gas, material injected from the CON and from the star-forming disk, as well as interstellar matter associated with the polar merger.
3. Na D interstellar absorption observed along the major axis does not participate in the rotation of the Zw 049.057 disk and kinematically resembles the gas observed in H I 21 cm absorption. The Na D absorption traces a reservoir of low angular momentum gas that could promote gas inflows to the center of the galaxy and thereby feed the CON.
4. High equivalent widths of the Hα and [N II] emission lines indicate a recent enhancement in star formation activity at ($r \gtrsim$300 pc) that also leads to injections of dusty gas to near kiloparsec heights above the disk plane. However, the disk SFR of $3\,M_\odot$ yr^{-1} from beyond the nuclear region does not suffice to contribute significantly to the $L_{\rm FIR} = 10^{11.5}\,L_\odot$ from Zw 049.057.
5. Two distinctive linear "dust pillars" extend from the region of the CON to kiloparsec heights above the disk. Pillar-1 originates from the projected position of the CON while Pillar-2, which lies close to the galaxy's minor axis, is offset from Pillar-1 by about 100 pc in projection as well as in angle and depth along the line of sight. Pillar-1 has properties of a collimated outflow coming from the CON. Pillar-2 could arise from a curved outflow from the CON, a second unobserved nucleus, or the compressed wall formed by the fast nuclear molecular outflow. The collimated outflow model for pillars gives mass flow rates from the CON region of $>2\,M_\odot$ yr^{-1}. Independent of the specifics of their origins, dust pillars are optically visible signatures of ongoing large-scale mechanical and mass feedback from the hidden CON in Zw 049.057. The presence of dust pillar absorption features emanating from galaxy nuclear regions offers a way to find candidate CONs via optical imaging.

6. The termination of both dust pillars into more diffuse structures within heights of $\lesssim$1 kpc indicates that gas ejected from the nuclear region does not readily escape the galaxy. Confinement of ejected gas to the inner galaxy is favorable for gas recycling between the CON and the wider ISM. A minimum CON lifetime of 3 Myr comes from our estimates of flow times along the dust pillars, while the maximum CON lifetime is not constrained.
7. The region within $r \approx$100 pc of the CON provides most of the luminosity from Zw 049.057. The compact size and radio properties of the CON suggest the presence of a powerful central AGN, possibly in combination with intense, compact star formation. The powerful nuclear region contains only a small fraction of the galaxy's stellar mass, leading to the low $M_*/L_{\rm FIR} = 0.05$ in Zw 049.057. A low $M_*/L_{\rm FIR}$ ratio is potentially a useful marker for the presence of candidate CONs in LIRGs.
8. If young stars are a significant power source in the CON, then an SFR of $\sim 20\,M_\odot$ yr^{-1} is required to produce most of the observed $L_{\rm FIR}$ from Zw 049.057. Such a high SFR would lead to rapid growth of a massive stellar complex within an $r \lesssim 100$ pc radius region and rapid depletion of the CON's gas supply.
9. Radiation pressure on dust can be a factor in CONs. In the case of a spherical dust distribution, radiation pressure limits the SMBH Eddington factor and maximum luminosity of the AGN to levels well below the observed $L_{\rm FIR}$. This constraint could be overcome by the gravitation from a dust-enveloped SMBH with $M_{\rm SMBH} \sim 10^8\,M_\odot$, that would be unusually massive for a galaxy like Zw 049.057, or by a CON structure such that a central AGN avoids the radiation pressure limit. In either of these two cases, the SMBH then could accrete with a high Eddington factor thereby enabling the AGN to provide much of $L_{\rm FIR}$ for Zw 049.057, and possibly promoting substantial growth if the SMBH has a mass in the $10^6\,M_\odot$ range .

Acknowledgments

We thank our colleagues and especially Kazushi Sakamoto and Nick Scoville for informative discussions of CONs and their relationships to properties of Zw 049.057. Our appreciation goes to Françoise Combes for providing important suggestions for improving the manuscript and to the referee for helpful reviews. Based on observations made with the NASA/ESA Hubble Space Telescope, obtained from the Data Archive at the Space Telescope Science Institute, which is operated by the Association of Universities for Research in Astronomy, Inc., under NASA contract NAS 5-26555. These observations are associated with program No. HST-GO-14728. Support for program HST-GO-14728 was provided by NASA through a grant from the Space Telescope Science Institute, which is operated by the Association of Universities for Research in Astronomy, Inc., under NASA contract NAS 5-26555. J.S.G., J.K., and L.L. are also thankful for funding of this research provided by the University of Wisconsin-Madison College of Letters and Science. R.K. gratefully acknowledges partial funding support from the National Aeronautics and Space Administration under project 80NSSC18K1498, and from the National Science Foundation under grant Nos. 1852136 and 2150222. E.G. gratefully acknowledges funding support from the National Science Foundation under grant No. 1852136. S.A., S.K., and C.W. gratefully acknowledge funding from the European Research Council (ERC) under the European Union's Horizon 2020 research and innovation program (grant agreement No. 789410). Some of the observations reported in this paper were obtained with the Southern African Large Telescope under program 2018-2-SCI-31 (PI: J. Gallagher). The NSF's NOIRLab is operated by the Association of Universities for Research in Astronomy (AURA) under a cooperative agreement with the National Science Foundation. Database access and other data services are provided by the Astro Data Lab. The Legacy Surveys consist of three individual and complementary projects: the Dark Energy Camera Legacy Survey (DECaLS; NOAO Proposal ID 2014B-0404; PIs: David Schlegel and Arjun Dey), the Beijing-Arizona Sky Survey (BASS; NOAO Proposal ID 2015A-0801; PIs: Zhou Xu and Xiaohui Fan), and the Mayall z-band Legacy Survey (MzLS; NOAO Proposal ID 2016A-0453; PI: Arjun Dey). DECaLS, BASS, and MzLS together include data obtained, respectively, at the Blanco telescope, Cerro Tololo Inter-American Observatory, NSF's National Optical Infrared Astronomy Research Laboratory (NOIRLab); the Bok telescope, Steward Observatory, University of Arizona; and the Mayall telescope, Kitt Peak National Observatory, NOIRLab. The Legacy Surveys project is honored to be permitted to conduct astronomical research on Iolkam Du'ag (Kitt Peak), a mountain with particular significance to the Tohono O'odham Nation. This research has made use of the NASA/IPAC Infrared Science Archive, which is funded by the National Aeronautics and Space Administration and operated by the California Institute of Technology. The National Radio Astronomy Observatory is a facility of the National Science Foundation operated under cooperative agreement by Associated Universities, Inc.

Software: python (Astropy Collaboration et al. 2013), saoimage ds9 (Joye & Mandel 2003), pySALT (Crawford 2017), IRAF (Tody 1986, 1993).

Facilities: SALT, HST, MAST, IRSA, NED, ADS

ORCID iDs

J. S. Gallagher https://orcid.org/0000-0001-8608-0408
R. Kotulla https://orcid.org/0000-0002-4460-9892
L. Laufman https://orcid.org/0000-0002-2121-5137
S. Aalto https://orcid.org/0000-0002-5828-7660
N. Falstad https://orcid.org/0000-0001-7593-1705
G. C. Privon https://orcid.org/0000-0003-3474-1125
A. Evans https://orcid.org/0000-0003-2638-1334

References

Aalto, S., Martín, S., Costagliola, F., et al. 2015, A&A, 584, A42
Aalto, S., Costagliola, F., Muller, S., et al. 2016, A&A, 590, A73
Aalto, S., Muller, S., König, S., et al. 2019, A&A, 627, A147
Aalto, S., Falstad, N., Muller, S., et al. 2020, A&A, 640, A104
Alatalo, K., Davis, T. A., Bureau, M., et al. 2013, MNRAS, 432, 1796
Alatalo, K., Nyland, K., Graves, G., et al. 2014, ApJ, 780, 186
Alonso-Herrero, A., Rieke, G. H., Rieke, M. J., et al. 2006, ApJ, 650, 835
Arnaboldi, M., Capaccioli, M., Cappellaro, E., Held, E. V., & Sparke, L. 1993, A&A, 267, 21
Astropy Collaboration, Robitaille, T. P., Tollerud, E. J., et al. 2013, A&A, 558, A33
Baan, W. A., An, T., Klöckner, H.-R., & Thomasson, P. 2017, MNRAS, 469, 916
Baan, W. A., Henkel, C., & Haschick, A. D. 1987, ApJ, 320, 154

Baan, W. A., Henkel, C., Loenen, A. F., Baudry, A., & Wiklind, T. 2008, A&A, 477, 747
Baba, S., Imanishi, M., Izumi, T., et al. 2022, ApJ, 928, 184
Baron, D., Netzer, H., Davies, R. I., & Xavier Prochaska, J. 2020, MNRAS, 494, 5396
Bergvall, N., Marquart, T., Way, M. J., et al. 2016, A&A, 587, A72
Boettcher, E., Gallagher, J. S. I., & Zweibel, E. G. 2019, ApJ, 885, 160
Boettcher, E., Gallagher, J. S. I., Ohyama, Y., et al. 2020, A&A, 637, A17
Boizelle, B. D., Barth, A. J., Darling, J., et al. 2017, ApJ, 845, 170
Bournaud, F., Jog, C. J., & Combes, F. 2005, A&A, 437, 69
Buckley, D. A. H., Barnes, S. I., Burgh, E. B., et al. 2008, Proc. SPIE, 7014, 701407
Calzetti, D. 1997, AJ, 113, 162
Calzetti, D. 2001, PASP, 113, 1449
Calzetti, D., Battisti, A. J., Shivaei, I., et al. 2021, ApJ, 913, 37
Cazzoli, S., Arribas, S., Maiolino, R., & Colina, L. 2016, A&A, 590, A125
Chandar, R., Caputo, M., Linden, S., et al. 2023, ApJ, 943, 142
Condon, J. J., Cotton, W. D., Greisen, E. W., et al. 1998, AJ, 115, 1693
Cortijo-Ferrero, C., González Delgado, R. M., Pérez, E., et al. 2017, A&A, 607, A70
Costagliola, F., Sakamoto, K., Muller, S., et al. 2015, A&A, 582, A91
Crawford, S. M. 2017, in ASP Conf. Ser. 512, Astronomical Data Analysis Software and Systems XXV, ed. N. P. F. Lorente, K. Shortridge, & R. Wayth (San Francisco, CA: ASP), 375
Crawford, S. M., Still, M., Schellart, P., et al. 2010, Proc. SPIE, 7737, 773725
Donnan, F. R., Rigopoulou, D., García-Bernete, I., et al. 2023, A&A, 669, A87
Downes, D., & Solomon, P. M. 1998, ApJ, 507, 615
Draine, B. T. 2011, Physics of the Interstellar and Intergalactic Medium (Princeton, NJ: Princeton Univ. Press)
Eliche-Moral, M. C., Rodríguez-Pérez, C., Borlaff, A., Querejeta, M., & Tapia, T. 2018, A&A, 617, A113
Evans, A. S., Becklin, E. E., Scoville, N. Z., et al. 2003, AJ, 125, 2341
Falstad, N., González-Alfonso, E., Aalto, S., et al. 2015, A&A, 580, A52
Falstad, N., Aalto, S., Mangum, J. G., et al. 2018, A&A, 609, A75
Falstad, N., Hallqvist, F., Aalto, S., et al. 2019, A&A, 623, A29
Falstad, N., Aalto, S., König, S., et al. 2021, A&A, 649, A105
Finkelman, I., Brosch, N., Funes, J. G., et al. 2012, MNRAS, 422, 1384
Fulmer, L. M., Gallagher, J. S., & Kotulla, R. 2017, A&A, 598, A119
Gallagher, J. S., & Hunter, D. A. 1981, AJ, 86, 1312
García-Bernete, I., Rigopoulou, D., Aalto, S., et al. 2022, A&A, 663, A46
George, K. 2017, A&A, 598, A45
Glass, D. H. W., Sansom, A. E., Davis, T. A., & Popescu, C. C. 2022, MNRAS, 517, 5524
González-Alfonso, E., & Sakamoto, K. 2019, ApJ, 882, 153
González-Alfonso, E., Pereira-Santaella, M., Fischer, J., et al. 2021, A&A, 645, A49
Gordon, K. D. 2021, in Star Formation Rates of Galaxies, ed. A. Zezas & V. Buat (Cambridge: Cambridge Univ. Press), 96
Gorski, M. D., Aalto, S., König, S., et al. 2023, A&A, 670, A70
Gorski, M. D., Aalto, S., König, S., et al. 2024, A&A, 684, L11
Greve, T. R., Leonidaki, I., Xilouris, E. M., et al. 2014, ApJ, 794, 142
Hattori, T., Yoshida, M., Ohtani, H., et al. 2004, AJ, 127, 736
Haynes, M. P., Giovanelli, R., Kent, B. R., et al. 2018, ApJ, 861, 49
Herrero-Illana, R., Privon, G. C., Evans, A. S., et al. 2019, A&A, 628, A71
Holmberg, E. 1958, MeLuS, 136, 1
Howk, J. C., & Savage, B. D. 1997, AJ, 114, 2463
Imanishi, M., & Nakanishi, K. 2013, AJ, 146, 91
Ishibashi, W., Fabian, A. C., & Maiolino, R. 2018, MNRAS, 476, 512
Janz, J., Norris, M. A., Forbes, D. A., et al. 2016, MNRAS, 456, 617
Joye, W. A., & Mandel, E. 2003, in ASP Conf. Ser. 295, Astronomical Data Analysis Software and Systems XII, ed. H. E. Payne, R. I. Jedrzejewski, & R. N. Hook (San Francisco, CA: ASP), 489
Józsa, G. I. G., Oosterloo, T. A., Morganti, R., Klein, U., & Erben, T. 2009, A&A, 494, 489
Kamenetzky, J., Rangwala, N., & Glenn, J. 2017, MNRAS, 471, 2917
Kannappan, S. J. 2004, ApJL, 611, L89
Karademir, G. S., Remus, R.-S., Burkert, A., et al. 2019, MNRAS, 487, 318
Kaviraj, S., Ting, Y.-S., Bureau, M., et al. 2012, MNRAS, 423, 49
Keel, W. C., Maksym, W. P., Bennert, V. N., et al. 2015, AJ, 149, 155
Keel, W. C., Windhorst, R. A., Jansen, R. A., et al. 2023, AJ, 165, 166
Kennicutt, R. C., & Evans, N. J. 2012, ARA&A, 50, 531
Kotulla, R., Fritze, U., Weilbacher, P., & Anders, P., 2010 GALEV Evolutionary Synthesis Models, Astrophysics Source Code Library, ascl:1010.033
Krumholz, M. R., McKee, C. F., & Klein, R. I. 2005, ApJL, 618, L33
Kuiper, R., & Hosokawa, T. 2018, A&A, 616, A101
Kylafis, N. D., & Xilouris, E. M. 2005, in AIP Conf. Proc. 761, The Spectral Energy Distributions of Gas-Rich Galaxies: Confronting Models with Data, ed. C. C. Popescu & R. J. Tuffs (Melville, NY: AIP), 3
Laine, S., & Heller, C. H. 1999, MNRAS, 308, 557
Lankhaar, B., Aalto, S., Wethers, C., et al. 2024, arXiv:2406.07620
Larson, K. L., Sanders, D. B., Barnes, J. E., et al. 2016, ApJ, 825, 128
Lehmer, B. D., Alexander, D. M., Bauer, F. E., et al. 2010, ApJ, 724, 559
Leroy, A. K., Sandstrom, K. M., Lang, D., et al. 2019, ApJS, 244, 24
Li, Z., French, K. D., Zabludoff, A. I., & Ho, L. C. 2019, ApJ, 879, 131
Lu, N., Zhao, Y., Díaz-Santos, T., et al. 2017, ApJS, 230, 1
Luo, Y., Rowlands, K., Alatalo, K., et al. 2022, ApJ, 938, 63
Mangum, J. G., Darling, J., Henkel, C., & Menten, K. M. 2013a, ApJ, 766, 108
Mangum, J. G., Darling, J., Henkel, C., et al. 2013b, ApJ, 779, 33
Mangum, J. G., Darling, J., Menten, K. M., & Henkel, C. 2008, ApJ, 673, 832
Mapelli, M., Rampazzo, R., & Marino, A. 2015, A&A, 575, A16
Marcillac, D., Elbaz, D., Charlot, S., et al. 2006, A&A, 458, 369
Martin, C. L. 2005, ApJ, 621, 227
Martin, J. M., Bottinelli, L., Dennefeld, M., et al. 1988, A&A, 195, 71
Martín, S., Aalto, S., Sakamoto, K., et al. 2016, A&A, 590, A25
Matthews, L. D., & Gallagher, J. S. I. 2002, ApJS, 141, 429
Mihos, J. C., & Hernquist, L. 1994, ApJL, 425, L13
Mirabel, I. F., & Sanders, D. B. 1988, ApJ, 335, 104
Morganti, R., & Oosterloo, T. 2018, A&ARv, 26, 4
Natale, G., Popescu, C. C., Tuffs, R. J., & Semionov, D. 2014, MNRAS, 438, 3137
Nishimura, Y., Aalto, S., Gorski, M. D., et al. 2024, A&A, 686, A48
Oh, S. H., Kim, W.-T., Lee, H. M., & Kim, J. 2008, ApJ, 683, 94
Ohyama, Y., Sakamoto, K., Aalto, S., & Gallagher, J. S. I. 2019, ApJ, 871, 191
Osterbrock, D. E., Fulbright, J. P., Martel, A. R., et al. 1996, PASP, 108, 277
Papadopoulos, P. P., van der Werf, P. P., Xilouris, E. M., et al. 2012, MNRAS, 426, 2601
Pereira-Santaella, M., Alonso-Herrero, A., Colina, L., et al. 2015, A&A, 577, A78
Petric, A. O., Armus, L., Flagey, N., et al. 2018, AJ, 156, 295
Planesas, P., Mirabel, I. F., & Sanders, D. B. 1991, ApJ, 370, 172
Poggianti, B. M., & Wu, H. 2000, ApJ, 529, 157
Popescu, C. 2021, in Star Formation Rates of Galaxies, ed. A. Zezas & V. Buat (Cambridge: Cambridge Univ. Press), 204
Privon, G. C., Aalto, S., Falstad, N., et al. 2017, ApJ, 835, 213
Rathore, H., Kumar, K., Mishra, P. K., Wadadekar, Y., & Bait, O. 2022, MNRAS, 513, 389
Reines, A. E., Greene, J. E., & Geha, M. 2013, ApJ, 775, 116
Ricci, C., Trakhtenbrot, B., Koss, M. J., et al. 2017, Natur, 549, 488
Ricci, C., Ananna, T. T., Temple, M. J., et al. 2022, ApJ, 938, 67
Rosenberg, M. J. F., van der Werf, P. P., Aalto, S., et al. 2015, ApJ, 801, 72
Saglia, R. P., Sánchez-Blázquez, P., Bender, R., et al. 2016, A&A, 596, C1
Sakamoto, K., Aalto, S., Evans, A. S., Wiedner, M. C., & Wilner, D. J. 2010, ApJL, 725, L228
Sakamoto, K., Martín, S., Wilner, D. J., et al. 2021, ApJ, 923, 240
Sazonova, E., Alatalo, K., Rowlands, K., et al. 2021, ApJ, 919, 134
Scoville, N., Murchikova, L., Walter, F., et al. 2017, ApJ, 836, 66
Scoville, N. Z., Evans, A. S., Thompson, R., et al. 2000, AJ, 119, 991
Shabala, S. S., Ting, Y.-S., Kaviraj, S., et al. 2012, MNRAS, 423, 59
Smercina, A., Smith, J.-D. T., French, K. D., et al. 2022, ApJ, 929, 154
Sofue, Y., Wakamatsu, K.-I., & Malin, D. F. 1994, AJ, 108, 2102
Soifer, B. T., Sanders, D. B., Madore, B. F., et al. 1987, ApJ, 320, 238
Song, Y., Linden, S. T., Evans, A. S., et al. 2022, ApJ, 940, 52
Sparke, L. S., van Moorsel, G., Schwarz, U. J., & Vogelaar, M. 2009, AJ, 137, 3976
SSC & IRSA 2013, Spitzer Enhanced Imaging Products, IPAC, doi:10.26131/IRSA433
Stark, D. V., Kannappan, S. J., Wei, L. H., et al. 2013, ApJ, 769, 82
Stierwalt, S., Armus, L., Surace, J. A., et al. 2013, ApJS, 206, 1
Tenorio-Tagle, G., & Muñoz-Tuñón, C. 1998, MNRAS, 293, 299
Tody, D. 1986, Proc. SPIE, 627, 733
Tody, D. 1993, in ASP Conf. Ser. 52, Astronomical Data Analysis Software and Systems II, ed. R. J. Hanisch, R. J. V. Brissenden, & J. Barnes (San Francisco, CA: ASP), 173
Tran, H. D., Tsvetanov, Z., Ford, H. C., et al. 2001, AJ, 121, 2928
U, V., Sanders, D. B., Mazzarella, J. M., et al. 2012, ApJS, 203, 9
Varenius, E., Conway, J. E., Martí-Vidal, I., et al. 2014, A&A, 566, A15
Városi, F., & Dwek, E. 1999, ApJ, 523, 265
Venanzi, M., Hönig, S., & Williamson, D. 2020, ApJ, 900, 174
Wethers, C. F., Aalto, S., Privon, G. C., et al. 2024, A&A, 683, A27
White, R. E. I., Keel, W. C., & Conselice, C. J. 2000, ApJ, 542, 761
Yesuf, H. M., Faber, S. M., Trump, J. R., et al. 2014, ApJ, 792, 84